The Astrophysical Journal, 898:68 (16pp), 2020 July 20 https://doi.org/10.3847/1538-4357/ab9ec0

Properties of the KISS Green Pea Galaxies

Samantha W. Brunker[1], John J. Salzer[1], Steven Janowiecki[2], Rose A. Finn[3], and George Helou[4]
[1] Department of Astronomy, Indiana University, 727 East Third Street, Bloomington, IN 47405, USA; sbrunker@indiana.edu
[2] University of Texas at Austin, McDonald Observatory, TX 79734, USA
[3] Department of Physics, Siena College, 515 Loudon Road, Loudonville, NY 12211, USA
[4] Infrared Processing and Analysis Center, California Institute of Technology, Pasadena, CA 91125, USA
Received 2020 June 8; accepted 2020 June 18; published 2020 July 24

Abstract

Green peas (GPs) are a class of extreme star-forming galaxies (SFGs) at intermediate redshifts, originally discovered via color selection using multifilter, wide-field survey imaging data. They are commonly thought of as being analogs of high-redshift Lyα-emitting galaxies. The defining characteristic of GP galaxies is a high-excitation nebular spectrum with very large equivalent width lines, leading to the recognition that GP-like galaxies can also be identified in samples of emission-line galaxies. Here we compare the properties a sample of [O III]-selected SFGs ($z = 0.29$–0.41) from the KPNO International Spectroscopic Survey (KISS) with the color-selected GPs. We find that the KISS [O III]-selected galaxies overlap with the parameter space defined by the color-selected GPs; the two samples appear to be drawn from the same population of objects. We compare the KISS GPs with the full Hα-selected KISS SFG sample ($z < 0.1$) and find that they are extreme systems. Many appear to be young systems at their observed look-back times (3–4 Gyr), with more than 90% of their rest-frame *B*-band luminosity coming from the starburst population. We compute the volume density of the KISS red (KISSR) GPs at $z = 0.29$–0.41 and find that they are extremely rare objects. We do not see galaxies as extreme as the KISSR GPs in the local universe, although we recognize several lower-luminosity systems at $z < 0.1$.

Unified Astronomy Thesaurus concepts: Emission line galaxies (459); Galaxy abundances (574); Star formation (1569); Starburst galaxies (1570); Galaxy evolution (594)

1. Introduction

One of the foremost topics in modern extragalactic research is the ongoing attempt to understand the key physical processes that occurred during the era of reionization. During this period of time in the early universe, the intergalactic medium (IGM) went from being neutral and opaque for photons capable of ionizing hydrogen to ionized and transparent. Reionization appears to have been complete by $z \sim 6$ (e.g., Fan et al. 2006; McGreer et al. 2015), though determining exactly when it began is much less constrained and depends critically on the nature of the ionizing sources. Proposed candidates for the source of the ionizing radiation include star-forming galaxies (SFGs; e.g., Robertson et al. 2010), active galactic nuclei (AGNs; e.g., Haiman & Loeb 1998; Madau & Haardt 2015), and quasars (e.g., Madau et al. 2004).

The most commonly accepted narrative is that SFGs are the main contributors to reionization. This idea is complicated by the fact that star-forming regions are typically surrounded by large H I column densities that prevent the ionizing radiation produced by hot stars from escaping into the IGM. Low- and intermediate-mass galaxies may get around this problem if they have a fully ionized interstellar medium or one perforated by optically thin tunnels by which the ionizing radiation could escape (Jaskot & Oey 2013; Nakajima & Ouchi 2014; Rivera-Thorsen et al. 2015; Izotov et al. 2018b). The production and escape of ionizing radiation in SFGs is not yet fully understood, although major advances in the past 5–10 yr suggest that we are on the path toward a more complete understanding.

As it is difficult to observe high-redshift galaxies that leak Lyman-continuum radiation (LyC; $\lambda_{\rm rest} < 912$ Å), studies of lower-redshift LyC emitters are necessary in order to understand how ionizing radiation escapes from SFGs. A class of compact SFGs known as green peas (GPs; Cardamone et al. 2009) have become popular targets for these observations because of their apparent similarities to high-z SFGs (e.g., low metallicities and high specific star formation rates (sSFRs); Izotov et al. 2011; Nakajima & Ouchi 2014; Henry et al. 2015). A significant fraction of GPs show high Lyα escape fractions from 1% to 50% (e.g., Henry et al. 2015; Jaskot et al. 2017, 2019; Verhamme et al. 2017; Yang et al. 2017a; Izotov et al. 2020). The GPs also include some of the only known LyC-leaking SFGs in the local universe (e.g., Izotov et al. 2016a, 2016b, 2017, 2018a) and all of the systems with $f_{\rm esc}$(LyC) $> 5\%$. This makes GPs important systems for studying the escape mechanisms of ionizing radiation.

The GPs were originally discovered by citizen scientists as part of the Galaxy Zoo galaxy classification project. Following this discovery, Cardamone et al. (2009) published the first sample of GPs that were color-selected from the Sloan Digital Sky Survey (SDSS; York et al. 2000). However, this is not the only way to discover such objects. A key property of GPs is their extremely strong [O III] λ5007 emission lines. However, the SDSS color-based selection will only allow for the detection of GP-like objects in a restricted redshift range (see Section 3). More traditional emission-line selection methods (e.g., objective-prism/grism surveys, narrowband surveys) can allow for the discovery of GP-like objects over much broader redshift ranges (Hoyos et al. 2005; Kakazu et al. 2007). For example, a sample of GP-like galaxies was discovered via their [O III] emission lines as part of the KPNO International Spectroscopic Survey (KISS; Salzer et al. 2000, 2009). These [O III]-selected SFGs appear to have properties similar to the Cardamone et al. (2009) sample.

In the current study, we focus on three issues. First, are the KISS [O III]-selected emission-line galaxies (ELGs) truly analogous to the color-selected GP galaxies? We attempt to

answer this question by directly comparing the properties of the KISS objects with the Cardamone et al. (2009) GP sample. Second, we explore the nature and evolutionary status of the GP-like galaxies. Finally, we ask whether there are any GP galaxies in the very local ($z < 0.1$) universe and attempt to address the question of what the GPs seen at intermediate redshifts look like today. To address these latter two items, we utilize the full KISS catalog to create a local comparison sample of actively SFGs and look for nearby GP analogs.

In this paper, we present the properties of the KISS [O III]-detected SFGs. The sample selection and new observational data for the galaxies are presented in Section 2. The comparison of the KISS [O III]-detected sample with the Cardamone et al. (2009) sample is presented in Section 3. In Section 4 we compare the KISS [O III]-detected sample with the low-redshift KISS Hα-detected sample, as well as discuss the evolutionary status of the [O III]-detected galaxies. An analysis of the volume densities of the KISS [O III]-detected galaxies is presented in Section 5, and a discussion of GPs in the local universe is presented in Section 6. Our findings are summarized in Section 7.

All derived distance-dependent quantities assume a standard cosmology of $H_0 = 70$ km s^{-1} Mpc^{-1}, $\Omega_\Lambda = 0.73$, and $\Omega_M = 0.27$ throughout the paper.

2. The [O III]-selected KISS Galaxies

2.1. The KISSR ELGs

The GP-like galaxies being studied in the current paper were all discovered in KISS (Salzer et al. 2000). KISS employed a low-dispersion objective prism on the 0.61 m Burrell Schmidt[5] telescope on Kitt Peak to carry out a comprehensive survey of ELGs in the nearby universe. The objective-prism spectra covered two distinct wavelength ranges: $\lambda\lambda$6400–7200 Å (KISS red (KISSR), selected primarily by the Hα line; Salzer et al. 2001; Gronwall et al. 2004b; Jangren et al. 2005a) and $\lambda\lambda$4800–5500 Å (KISS blue (KISSB), selected primarily by the [O III] λ5007 line; Salzer et al. 2002). All of the GP-like galaxies were detected in the KISSR portion of the survey.

A program of "quick-look" follow-up spectroscopy was carried out by members of the KISS collaboration. These spectra were used for determining accurate redshifts and ascertaining the activity type of each galaxy (e.g., star-forming versus AGN). Spectroscopic observations for the KISS ELGs are presented in Wegner et al. (2003), Gronwall et al. (2004a), Jangren et al. (2005b), and Salzer et al. (2005b); additional unpublished spectral data also exist. See Hirschauer et al. (2018) for a recent summary of the full spectroscopic follow-up of KISS. All 2157 KISSR ELGs from the first two survey catalogs (Salzer et al. 2001; Gronwall et al. 2004b, hereafter KR1 and KR2, respectively) possess follow-up spectra. The current study focuses primarily on the galaxies in the KR1 and KR2 lists.

The vast majority of the KISSR galaxies were detected via the Hα emission line, resulting in a sample of ELGs with redshifts between 0.0 and 0.095 (limited by the survey filter). However, roughly 2% were detected by strong [O III] λ5007 emission that was redshifted into the KISSR filter bandpass. These objects, which have redshifts between 0.29 and 0.42, tend to have large equivalent width (EW) emission lines and high excitation (large [O III]/Hβ) values.

In a preliminary analysis, Salzer et al. (2009) found that 15 of the 38 [O III]-detected KISSR ELGs were star-forming systems based on their locations in line diagnostic diagrams (e.g., Baldwin et al. 1981; Veilleux & Osterbrock 1987); the remaining [O III] detections were all AGNs, mainly Seyfert 2 galaxies. Two of the star-forming KISSR galaxies (KISSR 169 and 980) do not have characteristics that mimic the GP galaxies and are not discussed further in this study.

Most of the [O III]-detected SFGs possessed high-excitation spectra that were reminiscent of dwarf SFGs despite their high luminosities ($M_B \sim -20$ to -22). Using a strong line metallicity indicator (e.g., Melbourne & Salzer 2002; Salzer et al. 2005a), Salzer et al. (2009) showed that the [O III]-detected KISSR ELGs were located more than a factor of 10 below local SFGs in a metallicity–luminosity diagram. None of the spectra available at that time were of sufficient quality to allow for the derivation of direct abundances.

We illustrate the spectral characteristics of the KISSR [O III]-detected SFGs in Figure 1. These spectra were recently obtained as part of a study to measure accurate metallicities of the KISS GP-like galaxies (S. W. Brunker et al. 2020, in preparation). Compared to the KISS quick-look spectra described above, these data possess substantially higher signal-to-noise ratios and, in many cases, will allow the derivation of direct abundances. The presence of the [O III] λ4363 temperature-sensitive auroral line is clearly visible in all of the examples shown. It is worth stressing that the KISSR [O III]-detected galaxies have spectra reminiscent of the the GP galaxies (e.g., Cardamone et al. 2009; Izotov et al. 2011).

2.2. New IR Observations and Derivation of Stellar Masses

The mass of the stellar component of a galaxy is a key parameter for interpreting its nature. Traditional methods for deriving stellar masses include (1) using optical luminosities and colors combined with modeled mass-to-light ratios (M/L) and (2) spectral energy distribution (SED) fitting using optical broadband magnitudes (Bell & de Jong 2001; Bell et al. 2003a; Walcher et al. 2011). However, for systems with intense star formation, such as the ones in the current study, these standard mass-estimation methods can be highly inaccurate. This is true for two reasons. First, in extreme starbursts, the optical broadband luminosities can be enhanced by huge amounts due to the luminous young stars. The population of newly formed stars often contributes very little to the total stellar mass despite dominating the light output. Second, nebular line emission can dramatically change the broadband colors of these galaxies (case in point: the GPs). Since the simple M/L prescriptions used in method (1) above are based on stellar emission alone, this can lead to large discrepancies. In such cases, the best approach to deriving reliable stellar masses involves utilizing observations in the near-IR (NIR), where the contribution from the young stars does not dominate so severely.

In order to provide better determinations of the stellar masses for the [O III]-detected KISSR galaxies, we have undertaken new observations. These new data include both ground-based NIR imaging and space-based mid-IR (MIR) and far-IR (FIR) observations with the Spitzer Space Telescope.

None of the star-forming [O III]-detected KISSR galaxies are bright enough to have been detected by the Two Micron All

[5] The Burrell Schmidt telescope of the Warner and Swasey Observatory is operated by Case Western Reserve University.

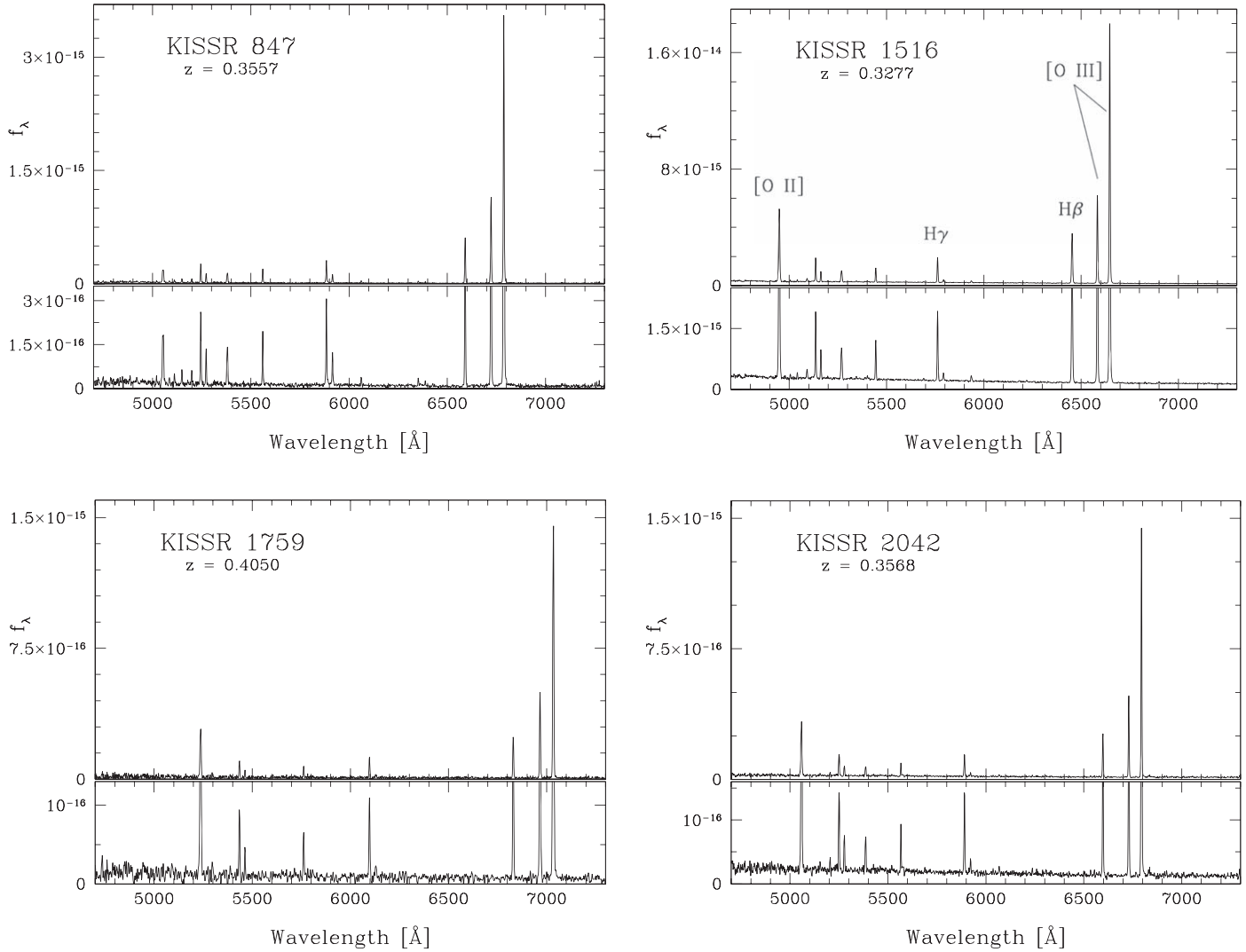

Figure 1. Spectra of four KISSR GP-like galaxies. Key emission lines are labeled in the upper right spectrum. All exhibit the strong [O III] $\lambda\lambda$5007, 4959 lines characteristic of the GP galaxies. KISSR 847 (upper left) is extreme in all aspects, exhibiting very high EW [O III] lines but very weak [O II] $\lambda\lambda$3729, 3726. The lower subpanel of each spectrum shows a clipped version of the y-axis in order to allow the reader to see the weaker emission lines, including [O III] λ4363 just redward of Hγ. We also possess spectra that reach redward to the location of the Hα and [N II] lines (not shown) that allow us to confirm the star-forming nature of these galaxies.

Sky Survey (Skrutskie et al. 2006). Therefore, we carried out NIR imaging observations using the WIYN High-resolution InfraRed Camera (WHIRC; Meixner et al. 2010) on the WIYN[6] 3.5 m telescope. The observational methods and data reduction procedures mirror those described in Janowiecki & Salzer (2014). In total, 11 of the 13 [O III]-detected KISSR galaxies were observed in both the J (1.25 μm) and H (1.65 μm) filters, while the remaining two were observed only in H. Our NIR magnitudes for the KISSR [O III]-detected galaxies are listed in Table 1.

Seven of the KISSR [O III]-detected SFGs were observed with the Spitzer Space Telescope[7] using both the IRAC (3.6, 4.5, 5.7, and 7.9 μm) and MIPS (24 and 70 μm) instruments. The observations were carried out in 2009 as part of a Director's Discretionary Time request; the objects selected for observation were chosen to cover the range of observed optical luminosities. We used the MOsaicker and Point source EXtractor (MOPEX) software tool[8] to reduce both the IRAC and MIPS data. For the IRAC data, we followed the the Spitzer Data Analysis Cookbook for "Point Source Photometry from IRAC Images."[9] We applied an array-dependent photometric correction to the corrected basic calibration data (CBCD) images because our sources are blue. We used the Astronomical Point Source EXtraction (APEX) software to perform point-source fitting on individual images using APEX multiframe point-source extraction mode, and we used a point response function (PRF) map provided by the Spitzer Space Center. We used the total flux from APEX.

For the MIPS 24 μm imaging, we created the image mosaics following the reduction procedure outlined in Finn et al. (2010) and the Spitzer Data Analysis Cookbook for "MIPS

[6] The WIYN Observatory is a joint facility of the University of Wisconsin–Madison, Indiana University, the University of Missouri, Purdue University, and the National Optical Astronomy Observatory.

[7] This work is based in part on observations made with the Spitzer Space Telescope, which was operated by the Jet Propulsion Laboratory, California Institute of Technology, under a contract with NASA.

[8] https://irsa.ipac.caltech.edu/data/SPITZER/docs/dataanalysistools/tools/mopex/

[9] https://irsa.ipac.caltech.edu/data/SPITZER/docs/dataanalysistools/cookbook/12/

Table 1
New NIR and Spitzer Observations of the KISSR [O III]-detected Galaxies

KISSR	J (mag)	H (mag)	IRAC 3.6 (mJy)	IRAC 4.5 (mJy)	IRAC 5.7 (mJy)	IRAC 7.9 (mJy)	MIPS 24 (mJy)	MIPS 70 (mJy)
(1)	(2)	(3)	(4)	(5)	(6)	(7)	(8)	(9)
225	18.31 ± 0.04	17.53 ± 0.04	75.4 ± 1.2	84.1 ± 1.6	78.0 ± 4.8	399.9 ± 10.4	1567 ± 33	11,930 ± 345
560	19.96 ± 0.16	18.67 ± 0.09	⋯	⋯	⋯	⋯	⋯	⋯
847	⋯	19.54 ± 0.23	22.2 ± 0.8	30.6 ± 1.3	43.2 ± 4.0	66.3 ± 8.7	567 ± 31	⋯
1038	19.40 ± 0.06	18.52 ± 0.06	28.6 ± 0.9	28.7 ± 1.2	41.4 ± 4.1	86.5 ± 8.2	1762 ± 28	14,060 ± 394
1290	18.76 ± 0.07	18.20 ± 0.06	⋯	⋯	⋯	⋯	⋯	⋯
1508	18.77 ± 0.07	17.99 ± 0.05	⋯	⋯	⋯	⋯	⋯	⋯
1516	18.60 ± 0.04	18.12 ± 0.05	54.1 ± 1.0	77.9 ± 1.5	96.3 ± 4.1	310.7 ± 9.0	4495 ± 30	24,400 ± 406
1759	20.15 ± 0.14	19.46 ± 0.10	40.3 ± 0.9	91.6 ± 1.6	243.7 ± 4.7	576.5 ± 9.6	2919 ± 29	9273 ± 296
1791	⋯	17.73 ± 0.13	⋯	⋯	⋯	⋯	⋯	⋯
1825	17.94 ± 0.04	16.96 ± 0.05	⋯	⋯	⋯	⋯	⋯	⋯
1953	18.68 ± 0.06	17.90 ± 0.04	49.6 ± 1.0	55.7 ± 1.4	56.2 ± 4.1	149.1 ± 8.8	2084 ± 29	18,120 ± 316
2005	18.69 ± 0.07	17.95 ± 0.08	⋯	⋯	⋯	⋯	⋯	⋯
2042	19.95 ± 0.08	19.45 ± 0.09	11.8 ± 0.7	11.2 ± 1.1	23.2 ± 4.3	⋯	302 ± 28	⋯

24 μm mosaic of a $z = 0.7$ cluster."[10] We flattened the basic calibration data (BCD) images and then created a mosaic with MOPEX. We extracted source photometry using APEX in single-frame point-source extraction mode, fitting the PRF in each image. Again, we use the total flux value calculated by APEX. The procedure for creating the mosaic and extracting fluxes was similar for the MIPS 70 μm images,[11,12] except that we started with the filtered BCD (FBCD) images that are available from the Spitzer archive. The FBCD images correct for striping that arises from differences in detector response, an effect that is not removed in the BCD images. The FBCD images yield reliable photometry for point sources with fluxes below 0.5 Jy, and they improved our ability to detect the KISS galaxies at 70 μm. The measured MIR and FIR fluxes for the seven KISSR [O III]-detected galaxies are listed in Table 1.

In addition to these new observations, the Wide-field Infrared Survey Explorer (WISE) all-sky survey (Wright et al. 2010) was sensitive enough to detect several of the KISSR [O III]-detected SFGs in one or more MIR bands (3.4, 4.6, 12, and 22 μm). All six of the KISSR [O III]-detected galaxies not observed by Spitzer were detected with WISE in at least one band, meaning that we have important NIR and MIR flux points for all of the [O III]-detected KISSR galaxy SEDs. For three KISSR galaxies with both Spitzer and WISE data, the agreement between the measured fluxes is quite good.

Detailed SED fits like those illustrated in Figure 2 were used to determine the stellar masses of these systems. We utilized the Code Investigating Galaxy Emission (CIGALE) software (Noll et al. 2009). CIGALE generates a grid of SEDs based on various theoretical models and compares with observed SEDs to determine the best values for each parameter in the models. Our wavelength coverage from UV to MIR (or, in some cases, FIR) allows CIGALE to self-consistently account for any dust absorption and reemission. Modules were employed that describe the nebular emission and absorption (Inoue 2011), dust attenuation (Cardelli et al. 1989), and thermal dust emission (Dale et al. 2014) using stellar population synthesis models (Bruzual & Charlot 2003) and a Salpeter (1955) initial mass function. Our fitting process and determination of stellar mass is more fully described in Appendix B of Hirschauer et al. (2018) and Section 3 of Janowiecki et al. (2017). We stress that the extreme star-forming nature of these types of systems makes the determination of accurate stellar masses extremely difficult. The inclusion of the NIR and MIR data is essential for constraining the stellar masses. We present our mass estimates in Table 2. Characteristic uncertainties in the mass determinations are 0.2–0.3 dex in $\log(M_*)$ (i.e., 30%–50% uncertainties in the mass).

Example broad wavelength coverage SEDs overplotted with the CIGALE model fits are illustrated in Figure 2. The data included in the SEDs range from the UV (Galaxy Evolution Explorer (GALEX) fluxes) to the FIR (Spitzer fluxes). The model fits include separate spectral plots for the stellar (orange) and dust (red) components. The nebular emission component is not plotted separately but is included in the composite model spectrum (black). The blue squares indicate the locations of measured fluxes for each galaxy. The locations of the squares vary from galaxy to galaxy, depending on the specific data set available for each galaxy.

2.3. Properties of the [O III]-detected KISSR Galaxies

We summarize the observed and derived characteristics of the KISS [O III]-detected SFGs in Table 2. Column 1 lists the KISSR number, while columns (2) and (3) give the equatorial coordinates of our galaxies (J2000). We note in passing that the decl. for KISSR 847 published in the original survey paper (Salzer et al. 2001) was incorrect; it corresponds to an $r = 17.15$ star located 13.″6 due N of KISSR 847. The coordinates listed here are the correct ones. Columns (4) and (5) list the B magnitude and $B - V$ color for each galaxy, corrected for Galactic absorption and reddening. The measured redshifts and [O III] EWs, derived from the KISS quick-look spectra, are given in columns (6) and (7). Formal uncertainties in the KISSR photometric and spectroscopic quantities listed here are included in the survey papers cited above.

The B-band absolute magnitudes are listed in column (8). These are observed, as opposed to rest-frame (i.e., K-corrected), luminosities; see the discussion in Section 4. Typical uncertainties are 0.1–0.2 mag. The median value of $M_B = -21.02$ for KISSR 1508 is somewhat brighter than M_B^*

[10] https://irsa.ipac.caltech.edu/data/SPITZER/docs/dataanalysistools/cookbook/28/
[11] https://irsa.ipac.caltech.edu/data/SPITZER/docs/dataanalysistools/cookbook/31/
[12] https://irsa.ipac.caltech.edu/data/SPITZER/docs/dataanalysistools/cookbook/34/

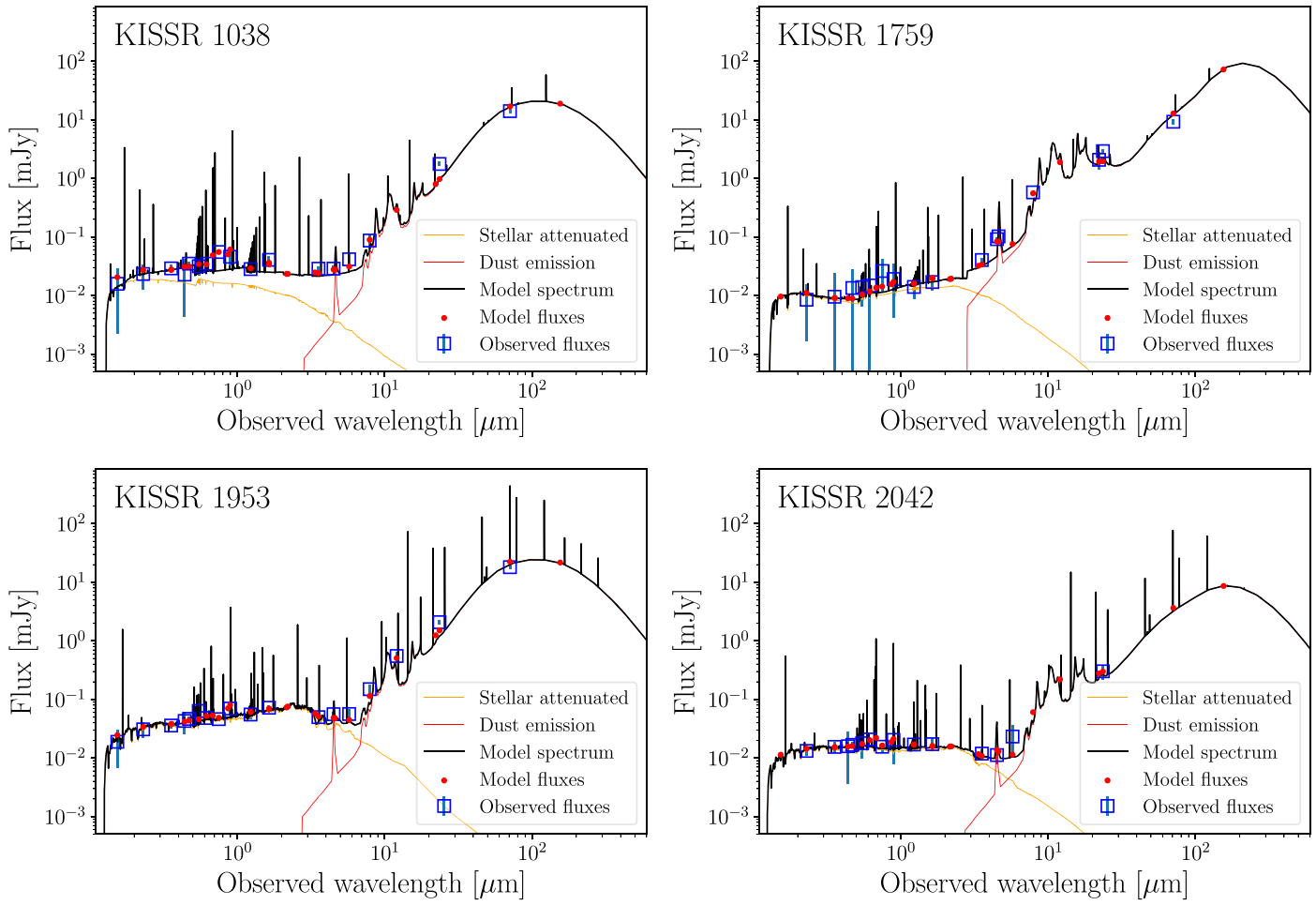

Figure 2. Observed SEDs and model fits for four [O III]-detected KISSR galaxies. The blue squares represent the locations of measured flux points, which range from the UV (GALEX FUV and NUV fluxes) to the FIR (Spitzer MIPS fluxes). The CIGALE model fits for the stellar component (orange curve), dust component (red curve), and composite model (stellar, dust, and nebular emission; black curve) are shown.

for the local B-band luminosity function (LF; approximately -20.0; Efstathiou et al. 1988; de Lapparent et al. 1989). However, the stellar masses listed in column (9) are more modest in scale. The median stellar mass of $M_* = 10^{9.55}\ M_\odot$, also for KISSR 1508, is lower than the characteristic mass determined from the stellar mass function ((1–2) $\times\ 10^{11}\ M_\odot$; Bell et al. 2003b; Panter et al. 2004). Oxygen abundances are listed in column (10). These values are derived using the O3N2 strong line method and have formal uncertainties of 0.10–0.15 dex (Hirschauer et al. 2018). Improved metallicities obtained using the direct method will be presented in S. W. Brunker et al. (2020, in preparation). Finally, column (11) presents the star formation rates (SFRs). These are derived using the Hα line fluxes and employ the standard Kennicutt (1998) SFR conversion factor (SFR $= L_{\rm H\alpha}/7.9 \times 10^{42}$). Typical uncertainties in the SFR values are $\sim$10%–20%, where the error is dominated by the uncertainty in the Hα flux measurement.

The derived properties of the KISSR [O III]-detected galaxies presented in Table 2 will be compared with similar quantities from samples of GP galaxies and local SFGs in the following sections.

3. KISSR [O III]-detected Galaxies as GPs

The KISSR [O III]-detected SFGs were cataloged using a very different selection method than that used in creating the GP galaxy sample (Cardamone et al. 2009), yet the spectra of the two sets of galaxies appear very similar. In the current section, we compare observed and derived quantities for the two samples of galaxies, with the goal of determining the extent to which the two groups can be thought of as forming one class of galaxies. The data for the GPs come from Cardamone et al. (2009), except for the oxygen abundances, which come from Izotov et al. (2011).

It is well understood that the observational characteristic that makes the GP galaxies green in the SDSS color images is the presence of a very strong [O III] λ5007 emission line that redshifts into the SDSS r-band filter (r is mapped to green in the SDSS color images). The redshift range of the Cardamone et al. (2009) GP galaxies is $0.141 < z < 0.348$ (see Figure 4). These redshifts nicely bracket the 50% throughput range of the SDSS r-band filter for the location of redshifted [O III] λ5007 (5710–6750 Å). At higher redshifts, the [O III] line is shifted out of the r band into the i band, so these objects no longer appear green in the color images and are not selected as GPs. Analogously, the redshift range of the [O III]-detected KISSR galaxies ($0.294 \leqslant z \leqslant 0.420$) is limited by the KISSR filter, which had a wavelength coverage of $\sim$6400–7200 Å (Salzer et al. 2000).

The impact of the combination of line strength and redshift is illustrated in Figure 3, which shows SDSS three-color images for three of the KISSR [O III]-detected galaxies. The two lower-

Table 2
Properties of KISSR [O III]-detected Galaxies

KISSR	R.A. (deg)	Decl. (deg)	B_o	$(B-V)_o$	z	EW$_{[O\,III]}$ (Å)	M_B	log(M_*) ($M_\odot$)	log(O/H)+12	log(SFR) ($M_\odot$ yr^{-1})
(1)	(2)	(3)	(4)	(5)	(6)	(7)	(8)	(9)	(10)	(11)
225	197.54067	29.29527	19.81	0.41	0.35822	102.4	−21.61	9.73	8.58	1.61
560	217.45028	29.48553	21.47	0.89	0.35787	405.7	−19.95	8.99	7.80	0.80
847	235.98020	29.46394	21.89	0.64	0.35575	1896.0	−19.52	8.86	7.65	1.36
1038	247.14056	29.32112	20.57	0.46	0.41001	731.1	−21.20	9.69	8.20	1.63
1290	185.60078	43.18965	20.13	0.58	0.30496	272.7	−20.89	9.44	8.25	0.97
1508	198.67200	43.72399	19.90	0.49	0.29397	413.1	−21.02	9.55	8.30	1.01
1516	198.95600	43.57503	19.51	0.15	0.32766	685.6	−21.69	9.67	8.17	1.32
1759	215.15889	43.72554	21.79	0.77	0.40504	1129.0	−19.95	9.32	7.97	1.02
1791	217.42047	43.90243	20.43	0.06	0.35923	213.1	−21.00	10.15	8.41	1.37
1825	219.08469	43.88378	19.56	0.27	0.33112	155.5	−21.67	10.25	8.60	1.26
1953	231.59900	43.00455	19.92	0.54	0.36882	427.2	−21.58	9.62	8.20	1.42
2005	235.69358	43.89937	20.02	0.26	0.30805	345.1	−21.03	9.10	8.46	1.31
2042	237.44008	43.05719	21.00	0.24	0.35680	953.2	−20.42	8.98	7.77	1.14

redshift systems, KISSR 1508 and KISSR 1516 (whose spectrum is shown in Figure 1), exhibit the characteristic green color seen in the Cardamone et al. (2009) GP galaxies. Both of these galaxies have redshifts that place the strong [O III] line in the SDSS r-band filter. However, the third galaxy shown, KISSR 1038, has a redshift that places the [O III] line in the SDSS i-band filter, which maps to red in the SDSS images. Presumably, it is the strong line emission in the SDSS i filter combined with the strong blue continuum emission in the SDSS g filter (mapped to blue) that gives rise to the strong purple hue seen in this galaxy.

The comparison of the redshifts of the two samples shown in Figure 4 reveals that there is substantial overlap. The KISSR [O III]-detected sample extends to somewhat larger redshifts, with the median redshift of 0.3568 lying just beyond the maximum redshift in the GP sample. This leads to the expectation that the KISSR [O III]-detected galaxies might be systematically higher-luminosity systems. As we see below, this expectation is at least partially borne out.

While the specific filters being used to create the two samples dictate the range of observed redshifts that can be detected, the key parameter that determines whether a galaxy will be selected as a GP or a KISS ELG is the emission-line strength. For both samples, it is a combination of the [O III] λ5007 line flux and the line EW that controls whether or not a source will be selected. Figure 5 shows the EW of the [O III] λ5007 line (EW$_{[O\,III]}$) versus the logarithm of the SFR for the KISSR [O III]-detected SFGs (red circles) and the Cardamone et al. (2009) GPs (green circles). The small black dots are the lower-redshift KISSR Hα-detected SFGs. In all cases, the SFR is derived from the measured Hα line luminosity assuming the Kennicutt (1998) conversion factor.

We highlight two important results illustrated in Figure 5. First, the KISSR [O III]-detected galaxies occupy the same region of the diagram as the Cardamone et al. (2009) GPs. This supports the hypothesis that the KISSR [O III]-detected galaxies are drawn from the same population of objects as the GPs. The KISSR [O III]-detected objects cover the same range of EW$_{[O\,III]}$ but tend to lie at the higher values of SFR (i.e., higher Hα luminosities). As alluded to above, the fact that the KISSR [O III]-detected galaxies are located at greater distances than the GPs means that they will preferentially sample the higher luminosities. Many of the Cardamone et al. (2009) GPs have SFRs lower than any of the [O III]-detected KISSR galaxies, but these tend to be located at smaller distances not covered by the KISSR [O III]-detected sample.

The second point to stress about the distributions shown in Figure 5 is the unique nature of the the GP galaxies. The small black dots represent ∼1390 Hα-detected SFGs in the local universe. They are from the deep, flux-limited KISSR sample. Yet there is virtually no overlap between the Hα-detected KISSR galaxies and the GPs. There are a number of KISSR galaxies with SFRs in the same range as the GPs, but none have EW$_{[O\,III]}$ values comparable to the GPs. Likewise, there are many Hα-detected KISSR galaxies with large EWs, but these all have lower SFRs. These are primarily star-forming dwarfs. Only a handful of the Hα-detected KISSR galaxies are located among the GPs in Figure 5, and these few are on the periphery of the distribution. Despite the fact that the Hα-detected portion of the KISSR sample has redshifts out to $z = 0.095$, there are no objects within the survey volume that have properties as extreme as the majority of the GP galaxies. We return to this point in the following sections.

Next, we plot the logarithm of the stellar mass (M_*) versus the logarithm of the sSFR (normalized by M_*) for the same three samples of SFGs in Figure 6. The same two trends we highlighted in Figure 5 are seen here. The Cardamone et al. (2009) GPs and KISSR [O III]-detected galaxies are colocated in the diagram, where again, the KISSR [O III]-detected galaxies are trending toward the extremes of the distribution. Once again, the GP galaxies are located in a region of the diagram that is largely devoid of examples from the low-redshift universe. Compared to Figure 5, there is somewhat more overlap between the samples in this figure, but nonetheless, the GPs are clearly seen to be extreme. The Hα-detected KISSR galaxies with sSFR values comparable to the GPs are lower-mass galaxies.

It is worth noting here that the GPs and KISSR GP-like galaxies possess a range of stellar mass values that span nearly 2 orders of magnitude, from $10^{8.5}$ to $10^{10.5}$ $M_\odot$. While some authors have referred to the population of GP galaxies as being dwarfs, it is clear that they actually span the full extent of intermediate masses and that the largest examples are quite massive.

Our last comparison of the KISSR samples with the Cardamone et al. (2009) GPs involves oxygen abundance and SFR. Figure 7 shows similar trends to the previous two plots. The GPs and KISSR [O III]-detected galaxies once again

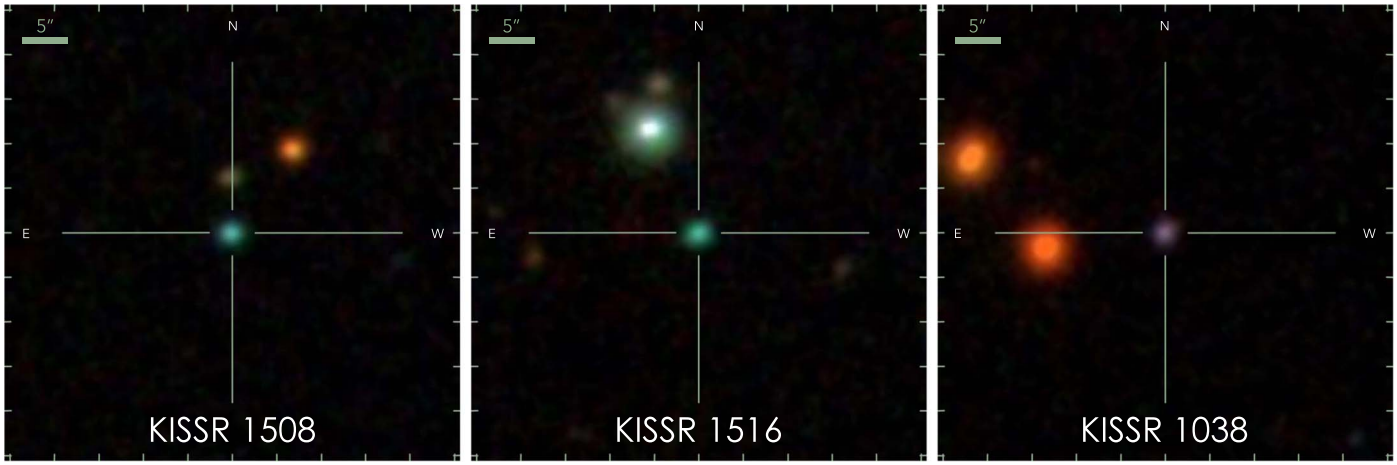

Figure 3. Images from SDSS of three of our [O III]-detected KISSR galaxies. Both KISSR 1508 and 1516 exhibit the green color for which the GP galaxies are known. These two ELGs have redshifts of 0.294 and 0.328, respectively, which places them in the same redshift range as the Cardamone et al. (2009) GPs (see Figure 4). However, KISSR 1038 ($z = 0.410$) appears violet in the SDSS three-color image because its strong [O III] line is redshifted out of the SDSS r filter and into the SDSS i filter (which maps to red in the SDSS RGB color images). Hence, higher-redshift GPs transition into purple grapes.

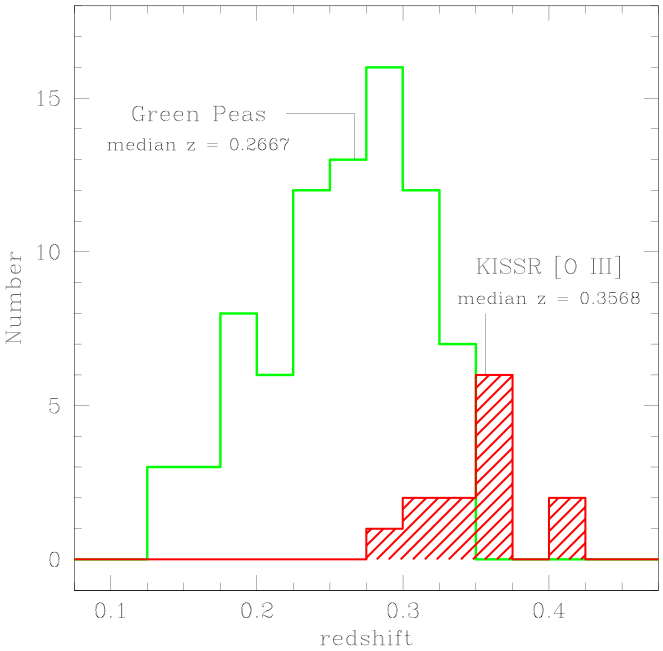

Figure 4. Redshift histograms for the Cardamone et al. (2009) GP galaxies (green histogram) and the KISSR [O III]-detected SFGs (red shaded histogram). The redshift ranges of the two samples are strongly defined by the selection methods used to detect the galaxies, as described in the text. The median KISSR redshift is slightly larger than the maximum redshift included among the Cardamone et al. (2009) GP galaxies ($z = 0.348$).

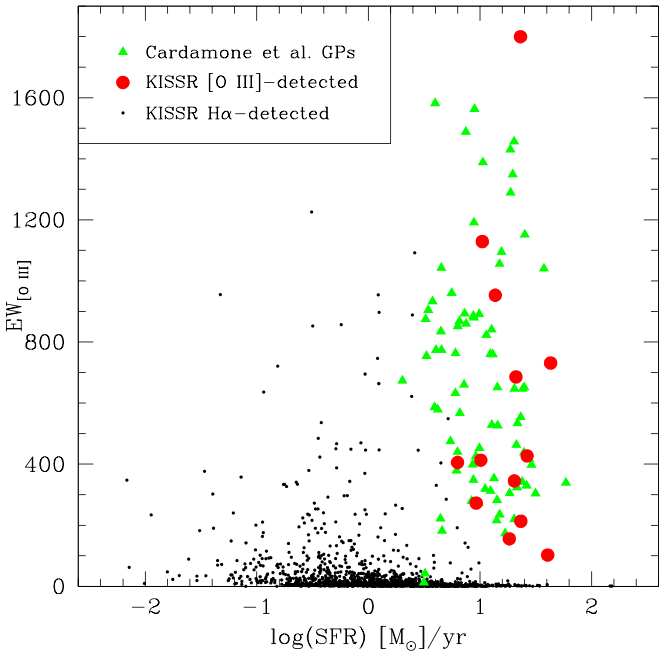

Figure 5. Observed [O III] λ5007 EW plotted against the SFR (derived from Hα line fluxes) for the Cardamone et al. (2009) GP galaxies (green dots), KISSR [O III]-detected SFGs (red dots), and KISSR Hα-detected SFGs (small black dots). The KISSR [O III]-detected galaxies occupy the same region as the GP galaxies: high SFR and large [O III] EWs. There is surprisingly very little overlap with the local KISSR Hα-detected sample, despite the fact that this survey goes out to $z = 0.095$ and detects the strongest SFGs within the local volume.

occupy the same region of parameter space. They are also almost completely offset from the KISS Hα-selected sample toward higher SFRs and/or lower abundances.

Figure 7 hints at another important characteristic of GPs and GP-like galaxies: they are metal-poor. When compared to galaxies with comparable SFRs, the GP galaxies exhibit, on average, nearly a full dex lower metallicities. We will return to this key feature in the next section.

Figures 4–7 tell a consistent story: the Cardamone et al. (2009) GPs and KISSR [O III]-detected SFGs have very similar properties. We conclude that the KISSR [O III]-detected galaxies are consistent with being drawn from the same population of extremely compact, high-SFR systems as the "classic" GPs. From this point on, we will refer to the KISSR [O III]-detected SFGs as the KISSR GPs.

4. Discussion: The Nature and Evolutionary Status of the KISSR GPs

Having established the similarities of the Cardamone et al. (2009) GPs and the KISSR [O III]-detected SFGs, we next switch our focus to trying to understand the nature of the KISSR GPs. Unfortunately, their substantial distances render studies involving morphology and physical size using our available ground-based data useless; the KISSR GPs are all

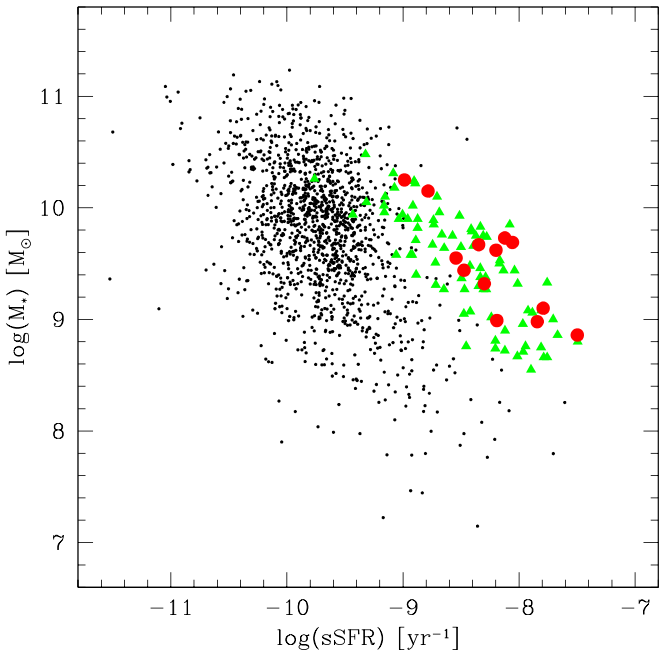

Figure 6. Stellar mass plotted vs. sSFR. The symbols have the same meaning as in Figure 5. The GP and [O III]-detected KISSR galaxies occupy a broad range of intermediate masses. They are quite distinct from the nearby Hα-selected SFGs, having extremely large sSFR values.

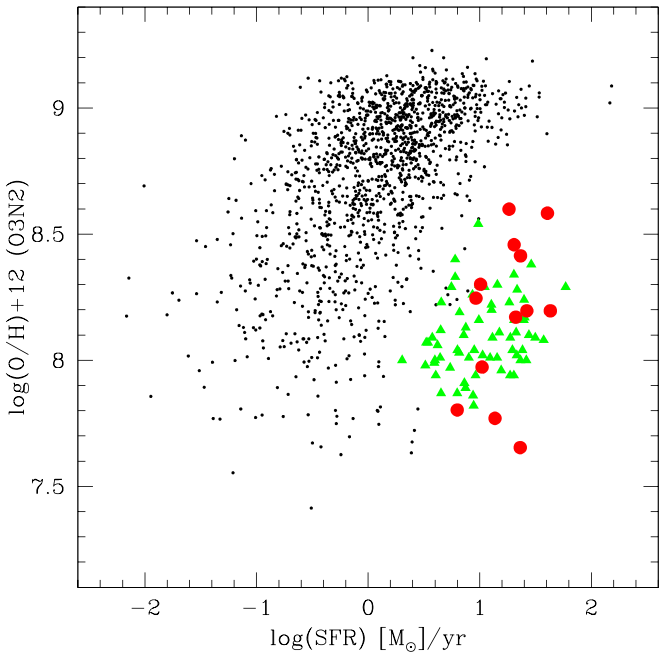

Figure 7. Oxygen abundance plotted against SFR. The symbols have the same meaning as in Figure 5. As in the previous figures, the GP and [O III]-detected KISSR galaxies show almost no overlap with the local SFGs.

unresolved in available images. Clearly, high-resolution space-based imaging would be highly useful in helping to understand the nature of these enigmatic objects. Nonetheless, we can make substantial progress in understanding these systems using the available data. This comparative study is aided by the availability of the large sample of lower-redshift Hα-detected KISSR galaxies.

We begin our efforts to place the KISSR GPs into context by looking at their optical luminosities. Figure 8 plots B-band

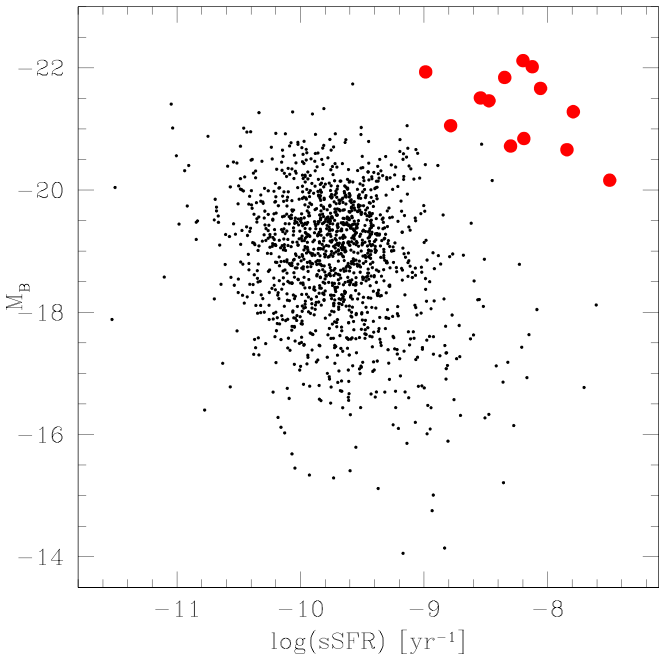

Figure 8. The B-band absolute magnitude plotted against the sSFR for the KISSR [O III]-detected (red dots) and Hα-detected (small black dots) SFGs.

absolute magnitude versus log(sSFR) for the KISS GPs (red dots) and the KISSR Hα-detected galaxies (small black dots). We note in passing that the Cardamone et al. (2009) study did not include an analysis of the optical luminosities of their GP sample, nor did they tabulate absolute magnitudes for their GPs. Hence, the Cardamone et al. (2009) GPs will not appear in the figures presented in this section of the paper.

In order to account for the redshift differences between the two samples, one would typically impose a "K correction" (Pence 1976; Hogg et al. 2002) on the light of one or both samples. However, the strongly starbursting nature of the KISSR GPs makes the implementation of standard K corrections inadequate. Rather, we need a correction that reflects the actual emission spectrum of these extreme objects. We get around this difficulty by recognizing that the redshifts of the two KISSR samples are such that the wavelength coverage of the Hα-detected KISSR galaxies in the B band is comparable to the wavelength coverage of the [O III]-detected KISSR galaxies as covered by the V band. In other words, we can simply substitute M_V for the KISSR GP galaxies for the comparison with M_B for the Hα-detected KISSR galaxies. This substitution is not perfect but to first order accounts for the redshift differences between the two samples. In Figure 8 and all subsequent figures utilizing B-band absolute magnitudes, the quantity being plotted for the KISSR GP galaxies is actually the measured V-band absolute magnitude M_V.

We stress that this is not a true K correction, since the corrected KISSR GP's absolute magnitudes are not rest-frame luminosities but rather shifted to match the average spectral bandpass of the KISSR Hα-detected galaxies. As long as the comparison is strictly between these two samples, however, the correction should be valid.

As seen in Figure 8, the KISS GPs are very luminous compared to the average galaxy in the KISS Hα-selected sample. The median (corrected) B-band absolute magnitude of the KISSR GPs is -21.5, roughly 1.5 mag above M_B^* for local galaxy samples (Efstathiou et al. 1988; de Lapparent et al.

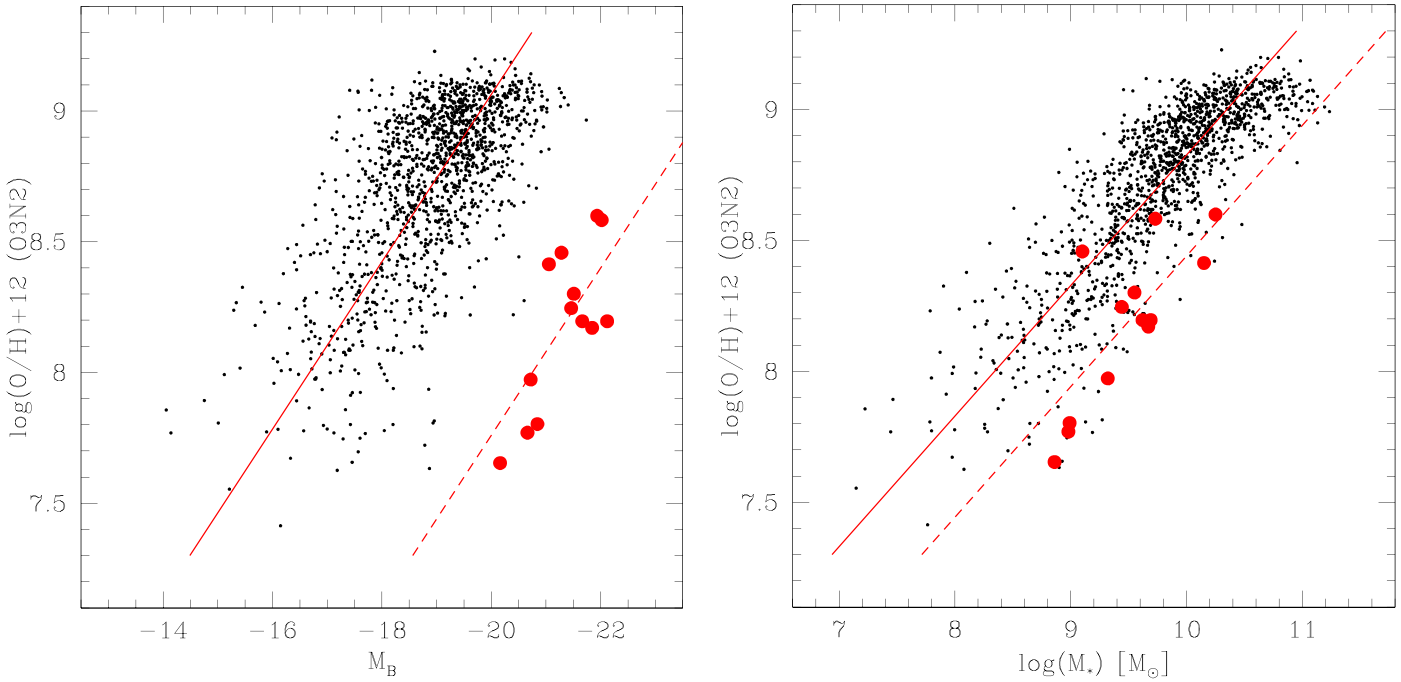

Figure 9. The LZ (left) and MZ (right) diagrams for the KISSR galaxies. The symbols have the same meaning as in Figure 8. In both panels, the solid red line is a bivariate linear least-squares fit to the low-redshift KISSR galaxies, adopted from Hirschauer et al. (2018). The dashed red lines are fits to the KISSR GPs, constrained to have the same slope as the fit to the low-z galaxies. The LZ diagram is similar to the one presented in Salzer et al. (2009) but uses updated abundances. The [O III]-selected galaxies are offset by a huge amount from the local SFGs. In the MZ diagram, the offset is still substantial but much reduced. This shows that the offset seen in the LZ plot is a combination of both abundance and luminosity offsets.

1989). As we saw previously, the KISS GPs have much larger values of log(sSFR) at a given mass/luminosity compared with the KISS Hα-selected sample. However, comparison with Figure 6 shows that the offset between the KISSR GPs and the KISSR Hα-detected sample is much more extreme when we substitute optical luminosity for mass. While the KISSR GPs lie in the middle of the range of stellar masses for the local KISSR galaxies, they are located at the very extreme end of the luminosity distribution. This is a strong indication of the strength of the starburst on the GP galaxies.

Important clues about the nature and evolutionary status of the KISSR GP galaxies can be inferred from their measured metallicities. All previous studies of GP-like galaxies have found that these objects have low oxygen abundances (e.g., Cardamone et al. 2009; Izotov et al. 2011). Salzer et al. (2009) presented a luminosity–metallicity (LZ) plot that showed that the [O III]-detected KISSR galaxies were located more than 1 dex below the LZ trend defined by the nearby Hα-detected KISSR galaxies. In that work, the offset between the two galaxy samples was interpreted as being primarily a metallicity offset. Here we show that this interpretation was too simplistic.

We present LZ and mass–metallicity (MZ) relations that compare the two galaxy samples in Figure 9. In both panels, the solid red line represents a bivariate linear least-squares fit to the low-redshift Hα-detected KISSR galaxies taken directly from Hirschauer et al. (2018). The dashed red lines are fits to the [O III]-detected KISSR galaxies, constrained to have the same slope as the fits to the Hα-selected galaxies. In the LZ relation shown in the left panel, the KISSR GPs do not overlap the KISSR Hα-detected sample at all. The vertical (metallicity) offset between the two fit lines is 1.30 dex, while the horizontal offset is 4.07 mag. We demonstrate below that the dramatic offset between the two samples is caused by a combination of an inherent metallicity offset and a strong luminosity enhancement due to the starburst.

The MZ relations are plotted in the right panel of Figure 9. Now the offset of the KISSR GPs from the KISSR Hα-detected sample is substantially reduced. By replacing luminosity with stellar mass on the horizontal axis, the luminosity enhancement due to the starburst is effectively removed. We argue that the remaining offset seen in the MZ plot is the intrinsic metallicity offset of the GPs relative to the nearby SFGs. The vertical offset between the two fits implies that the KISSR GPs are, on average, 0.39 dex lower metallicity. A few of the KISSR GPs (KISSR 225 and 2005) straddle the fit line for the low-redshift sample and are not metal-deficient at all. The remaining KISSR GPs fall within the lower envelope of galaxies in the MZ relation. They are clearly metal-poor for their masses but not as extreme as their appearance in the LZ diagram seemed to indicate.

A simple but effective way to quantify the strength of the starbursts on the KISSR GP galaxies is presented in Figure 10. Here we plot stellar mass against luminosity for both KISSR samples. In this figure, the horizontal offset between the two sets of galaxies directly measures the strength of the starburst in the GP galaxies. Based on the horizontal offset between the two fit lines (which are determined in the same way as the fits in Figure 9), we find that the average luminosity enhancement due to the starburst events in the GP galaxies is 3.08 mag (factor of 17 higher luminosity). We stress that this offset is measured relative to a population of actively SFGs whose own luminosities are enhanced by some amount. If measured against a population of quiescent galaxies, the starburst enhancement is likely to be even higher than measured here. It is also clear that the KISSR GPs exhibit a range of luminosity enhancements, from as low as 1.57 mag for KISSR 1791

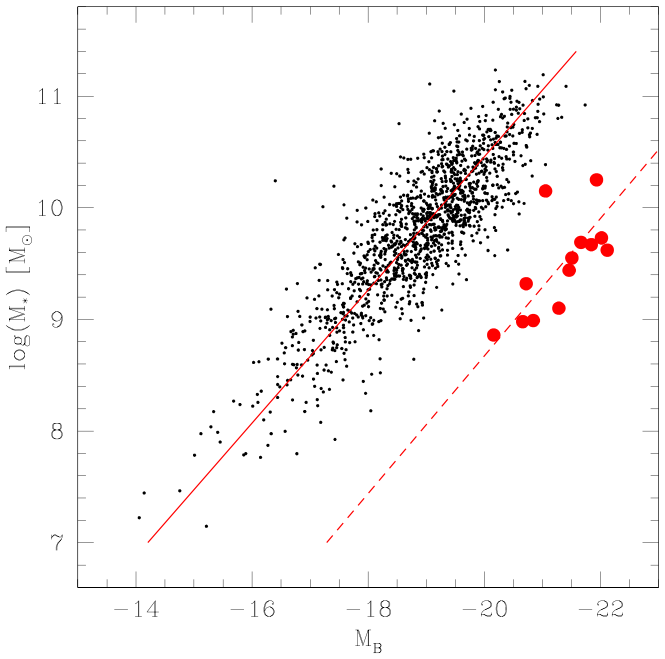

Figure 10. Stellar mass plotted against *B*-band absolute magnitude for the KISSR galaxies. The symbols have the same meaning as in Figure 8. The solid red line is a bivariate linear least-squares fit to the low-redshift KISSR galaxies, while the dashed red line is a fit to the KISSR GPs, constrained to have the same slope as the fit to the low-z galaxies. The luminosity enhancement for the [O III]-detected KISSR galaxies at a given mass is, on average, 3.08 mag (factor of 17).

(factor of 4 higher luminosity) to as high as 3.55 mag for KISSR 2005 (factor of 26 higher luminosity).

In the local universe, it is rare to find SFGs where more than half of the total light of the system is coming from the starburst population (e.g., Janowiecki & Salzer 2014). Such objects are typically blue compact dwarf galaxies with low luminosities and high sSFR values. There do not appear to be any examples in the nearby universe with star formation events as extreme as the GP galaxies. The average object in our sample is 17× more luminous in the *B* band than a typical local SFG of the same mass. This means that, on average, at least 94% of the *B*-band light from these systems must be coming from the starburst population, which in turn seems to imply that at least some of these systems are undergoing their first major episode of star formation.

Is it possible that the GP galaxies represent newly formed (or forming) systems? The current sample of GPs have look-back times of 3–4 Gyr. While the general picture of galaxy formation has most major galaxies forming at much higher redshifts, there is no reason why some of these intermediate-mass systems could not be coming together and having their first major star formation event at these late times.

An interesting parameter in this regard is the "star formation age" of these systems, obtained by dividing their stellar mass by their current SFR (i.e., just the inverse of the sSFR). The star formation age is the amount of time it would take to form the total stellar mass of the system at its current SFR. This must be considered to be a lower limit to their true ages, since we do not necessarily expect their high SFR rates to be sustainable over long periods of time. However, work by McQuinn et al. (2010) suggests that the lengths of starbursts in nearby low-mass galaxies can easily reach 500 Myr in duration. Based on the numbers in Table 2, the star formation ages of several of the KISSR GPs are extremely low: 31 Myr for KISSR 847, 62 Myr for KISSR 2005, and 70 Myr for KISSR 2042. In other words, these systems could form their entire mass of stars if they could sustain their current SFRs for several tens of millions of years. The median star formation age for our sample is 158 Myr, and 11 of the 13 galaxies have ages less than 350 Myr. Based on these numbers, it certainly seems possible that at least some of the KISSR GPs were young systems at the look-back times where we observe them.

We list parameters in Table 3 that illustrate the extreme nature of the KISSR GP galaxies. Column (2) gives the approximate *K*-corrected *B*-band absolute magnitude (i.e., the observed *V*-band absolute magnitude), while column (3) lists the starburst enhancement from Figure 10, defined as the horizontal offset of each GP galaxy from the trend line fit to the low-z KISSR galaxies. Column (4) converts this enhancement into the fraction of the *B*-band luminosity coming from the starburst population (stellar plus nebular emission). Column (5) lists the star formation age as defined above.

While the values exhibited in Table 3 are indeed extreme, they are confirmed and supported by the results of our SED model fitting described in Section 2.2. Even though our primary use of the CIGALE models for the current study has been to provide robust stellar mass determinations, the detailed SED fitting also generates estimates for several other key parameters (see Janowiecki et al. 2017, for details). Since the model results are based on the analysis of the full SED rather than an observation in a single passband (e.g., *B*-band magnitude or Hα line flux), they provide a largely independent measurement of the star-forming properties of the KISSR GPs. Two relevant examples from these models are included in Table 3.

Column (6) of Table 3 lists the birth-rate parameter b (Kennicutt 1983), defined as

$$b = \frac{\mathrm{SFR}_{\mathrm{current}}}{\langle \mathrm{SFR} \rangle}. \quad (1)$$

Here $\mathrm{SFR}_{\mathrm{current}}$ is the current SFR, where we use the modeled value for the SFR over the past 10 Myr, and $\langle \mathrm{SFR} \rangle$ is the lifetime average SFR. The burst mass fraction is given in column (7). This quantity is defined as the mass fraction of the young stellar population compared to the total stellar mass, where both are evaluated at the time of the initiation of the young population's formation burst.

The SED model results are in good general agreement with the observationally derived parameters listed in Table 3 and paint a similarly extreme picture of the nature of the starburst episodes of the KISSR GPs. A birth-rate parameter $b \gtrsim 3$ is generally adopted as an indicator that a strong starburst is occurring in a galaxy (e.g., Bergvall et al. 2016). All of the KISSR GPs have $b > 3$, and in fact, all but the two least severe systems (KISSR 1791 and 1825) have $b > 17$. Six of the KISSR GPs have burst mass fractions in excess of 50%; more than half of the stellar mass in these systems has been produced in the current burst. In the case of KISSR 847, the SED models indicate that more than 70% of the stellar mass was produced during the initial stages of the current starburst, which is broadly consistent with its extremely short star formation age of 31 Myr.

It is worth noting here that the extremely short star formation ages of the KISSR GPs are precisely one of the characteristics one looks for in a population of objects that could be

Table 3
The Extreme Nature of the KISSR [O III]-detected Galaxies

KISSR	Corrected M_B	Starburst Enhancement (mag)	Fraction of Light from Starburst (%)	Star Formation Age (Myr)	Birth-rate Parameter b	Burst Mass Fraction (%)
(1)	(2)	(3)	(4)	(5)	(6)	(7)
225	−22.02	3.24	94.9	133	24.2	52.3
560	−20.84	3.30	95.2	155	73.6	52.8
847	−20.16	2.84	92.7	31	69.9	70.4
1038	−21.67	2.95	93.4	114	17.9	8.3
1290	−21.46	3.16	94.6	298	31.8	51.5
1508	−21.51	3.03	93.9	349	35.7	30.9
1516	−21.84	3.16	94.6	222	23.8	10.5
1759	−20.72	2.62	91.0	199	74.2	57.9
1791	−21.06	1.57	76.4	608	3.3	8.6
1825	−21.93	2.28	87.8	971	6.1	4.7
1953	−22.12	3.52	96.1	158	19.8	13.3
2005	−21.28	3.55	96.3	62	113.7	56.1
2042	−20.66	3.13	94.4	70	27.4	35.2

contributing to the reionization of the universe. Current evidence suggests that reionization began at $z \sim 20$, when the universe was only ∼180 Myr old, and was largely complete by $z \sim 6$ (universe ∼950 Myr old). The short formation timescales implied by the star formation ages of the KISSR GPs would naturally allow the GP-like systems present in the early universe to be major contributors to the ionizing photons that were driving the reionization.

5. Number Densities of the [O III]-detected KISSR Galaxies

One of the strengths of the KISS sample of galaxies is that it represents a flux-limited catalog of ELGs with a well-defined selection function. As detailed in Gronwall et al. (2004b), the completeness of KISS is well parameterized by the emission-line fluxes measured from the digital objective-prism spectra. Each survey strip has a well-defined line-flux completeness limit that allows us to derive accurate volume densities for the KISS ELGs. This is in contrast to most existing samples of GP or GP-like galaxies (e.g., Cardamone et al. 2009; Izotov et al. 2011), where the samples were constructed either based on SDSS colors or by evaluation of existing SDSS spectra.

The line-flux completeness limit for the [O III]-detected KISSR galaxies will be the same as was derived for the full KISSR sample (e.g., Gronwall et al. 2004b), but the redshift range over which the GP-like galaxies can be detected is substantially different from that of the KISSR Hα-detected sample. Using the filter tracing of the KISSR survey filter (see Salzer et al. 2000), we determine that the [O III] λ5007 line would be detectable over the redshift range 0.290–0.422. We adopt these redshift limits to determine the maximum volume over which the [O III]-detected KISSR galaxies could be found. When coupled with the sky coverage of the two catalogs (62.162 deg^2 for KR1 and 65.864 deg^2 for KR2) and using the cosmology parameters specified in Section 1, these redshift ranges yield effective comoving volumes of 17.98×10^6 Mpc^3 for KR1 and 19.05×10^6 Mpc^3 for KR2.

Using the completeness limits for the KR1 and KR2 surveys together with the measured objective-prism line fluxes for the 13 KISSR [O III]-detected galaxies, we derive a comoving number density of 1.35×10^{-6} Mpc^{-3} for the KISSR GP galaxies. This value supersedes a preliminary value for the density of these galaxies presented in Salzer et al. (2009); the latter value is a factor of 3 smaller due to the simplifying assumptions used in its derivation.

In order to put this derived number density into context, we need to compare it to a comprehensive sample of galaxies located at a similar distance. The LF analysis presented in Faber et al. (2007) for the DEEP2 redshift survey provides an excellent comparison sample of galaxies. Faber et al. (2007) derived robust LFs for both the DEEP2 and Combo-17 data sets in a series of redshift intervals. We use their results for DEEP2 in the redshift range 0.2–0.4, which is a reasonable match for the redshift range of the KISSR GPs of 0.29–0.42. Integrating their derived LF for all galaxies over the M_B range −20.2 to −22.2 (i.e., the luminosity range of the KISSR GPs), we obtain a number density for the full galaxy population in this redshift range of 1.71×10^{-3} Mpc^{-3}. This is a factor of more than 1200 times larger than the number density of the KISSR GPs. Clearly, these GP-like galaxies are extremely rare, even at $z = 0.3$–0.4.

We utilize our derived number density for the KISSR GP-like galaxies in the following section, where we attempt to identify nearby examples of the GP galaxies.

6. Are There Local Analogs to the GPs?

Our discussion of the nature of the GPs presented in Section 4 paints a picture of an extreme population of galaxies that presumably evolves extremely rapidly from $z = 0.2$–0.4 to today. It raises a number of key questions. Do we see examples of the GPs in the very local universe ($z < 0.1$)? What do the extreme GPs seen in KISSR look like today? In this section, we explore these questions by utilizing both of the low-redshift KISS samples of strong ELGs: the Hα-detected KISSR galaxies and the [O III]-selected KISSB galaxies.

The question of whether we see GP galaxies in the local universe is at least partially answered by the Cardamone et al. (2009) study, which detects GPs at redshifts as low as 0.141 (see Section 3). Since their color-selection method imposes strict redshift limits on their sample, there is no reason to expect that similar objects would not be present at even lower redshifts. We note that the shape of the Cardamone et al. (2009) redshift histogram (Figure 4) may imply that GPs are less common at lower redshifts ($z < 0.225$) than at higher redshifts. The survey volume difference between the redshift bin with the

highest number of detections (0.275–0.30) and the bin at 0.15 exactly accounts for the difference in the number of detections. However, the nearer redshifts should be sensitive to lower-luminosity GPs, such that the expectations for detected sources in these bins would be higher than the predictions based purely on the geometry of the survey volume. Taken at face value, this seems to imply a fading of the GP population. Unfortunately, a more quantitative analysis would require a more precise definition of the selection function for the color-selected GP than is currently available.

On the other hand, Figures 5–7 reveal that there are no Hα-detected KISSR galaxies that overlap the properties of the [O III]-detected KISSR galaxies. While there are a handful of the lower-redshift KISSR galaxies that fall within the periphery of the Cardamone et al. (2009) GPs in these three figures (see below), none have properties that overlap with the higher-redshift KISSR galaxies. This does not necessarily imply that such extreme objects do not exist in the local universe, however. The volume density of the [O III]-detected KISSR GP-like galaxies (Section 5) combined with the effective volumes of the low-redshift portion of the KR1 and KR2 surveys ($\sim$520,000 Mpc^3) predicts that there should be 0.70 such galaxies within the Hα-detected portion of KISSR. Hence, the rarity of the extreme GPs represented by the KISSR [O III]-detected sample does not require even a single such object to be located within the Hα-detected KISSR catalog. However, wide-field redshift surveys like 2dF (Colless et al. 2001) and SDSS (Strauss et al. 2002) should have detected dozens of such objects with $z < 0.10$ if they exist in the local universe. We are not aware of any such detections.

In the following subsections, we utilize the full Hα-detected KISSR catalog to look for possible GP-like galaxies in the local universe.

6.1. Comparison with the Werk et al. LBCGs

A natural starting point for our search for GPs among the low-redshift KISS galaxies is to consider the properties of the KISS galaxies that have already been identified as being compact: the Werk et al. (2004) sample of luminous blue compact galaxies (LBCGs). For their study, Werk et al. (2004) used the same selection criteria proposed by Guzmán et al. (2003): surface brightness (B-band) < 21 mag arcsec^{-2}, $M_B < -18.5$, and $B - V < 0.6$. It is important to note that the Werk et al. (2004) LBCG sample is also redshift-limited ($z < 0.045$). This constraint was imposed due to the low resolution of the KISS survey images. In order to avoid including AGNs in the sample, Werk et al. (2004) also required that each galaxy selected as an LBCG have a follow-up spectrum that confirmed it as being star-forming. This is an additional limitation because the spectral follow-up for the KISS survey was far from complete in 2004.

To compare the properties of the Werk et al. (2004) LBCGs and our KISSR GPs, we followed the same procedure as in Section 3 when we compared the KISSR GPs to the Cardamone et al. (2009) GP sample. That is, we looked to see if the LBCGs overlap the combined parameter space of the KISSR and Cardamone et al. (2009) GPs. Figure 11 shows reproductions of Figures 5 and 6, with the Werk et al. (2004) LBCGs shown as black points enclosed in red circles.

Few of the LBCGs shown in Figure 11 reside in the same portion of parameter space as the GPs. There is nothing about the majority of the LBCGs that distinguishes them from the rest of the KISS Hα-selected SFGs; they have lower [O III] EW, SFR, and sSFR compared with the GPs. Most have EW$_{[O\ III]}$ less than 50 Å, which places them along the bottom of the left panel of Figure 11, while in the M_*–sSFR plot, they mix well with the rest of the Hα-detected KISSR galaxies.

There are two Werk et al. (2004) LBCGs that lie within the GP galaxy parameter space in Figure 11. These two galaxies, KISSR 242 and 1578, while located at the less extreme end of the GPs with regard to their properties, nonetheless still appear to qualify as GPs. However, when we look at their morphologies, we are immediately forced into the opposite conclusion. The GPs have a distinct semistellar morphology. Example images of some of the KISSR GPs are shown in Figure 3. The two LBCGs are shown in the leftmost images in Figure 12, and the differences in morphology are clear. The LBCGs are not compact in the same way as the GPs. The two LBCGs have a compact, high surface brightness region of star formation embedded in a larger, more extended galaxy. These two systems are most likely mergers. They are compact relative to the rest of the KISS Hα-selected SFGs, but they are much less compact than the KISSR GPs. We note that this apparent difference in morphology could be due in part to redshift and/or resolution differences of the samples; it may well be that the extended structures and tidal features of these LBCGs would be undetectable in ground-based images if these galaxies were viewed at redshifts of 0.3–0.4. However, we note that the other GP-like galaxies illustrated in Figure 11 (see Section 6.2) are located at distances of only a factor of $\sim$2 larger, yet they show no extended structures. The KISSR LBCGs are dramatically less compact than, for example, KISSR 1734, which has a similar stellar mass and SFR. Hence, we conclude that the list of Werk et al. (2004) LBCGs does not harbor any GP candidates.

6.2. Searching for GP Candidates in the Full KISS Sample

The evaluation of the KISS LBCGs did not result in the identification of any low-redshift GP-like objects. However, the approach allowed us to recognize that some SFGs exhibit many properties similar to the GP galaxies without being compact enough to allow them to be classified as such. Armed with this insight, we examined the properties of additional low-redshift KISSR and KISSB galaxies that happen to be located in the portion of parameter space occupied by the Cardamone et al. (2009) GP galaxies.

Our approach for trying to identify additional GP-like galaxies in the low-redshift portion of KISS was both simple and direct. We identified those KISS galaxies located in the region of overlap with the Cardamone et al. (2009) GPs in Figures 5–7 and having compact morphologies. The objects with blue circles in Figure 11, plus the LBCGs KISSR 242 and 1578 discussed in the previous subsection, were the only KISS galaxies that overlapped the parameters of the GPs in all three plots. As was already clear from our previous discussion, these low-redshift KISS galaxies are just barely overlapping the GPs; they are all found along the perimeter of the parameter space covered by the Cardamone et al. (2009) galaxies, having lower SFRs than most of the bona fide GPs.

When we evaluated the morphologies of these low-redshift GP candidates, we found that they fell into two distinct categories. Four of them were extremely compact and showed little or no extended structures outside of the bright central core. These four are illustrated in Figure 12: KISSR 715 and

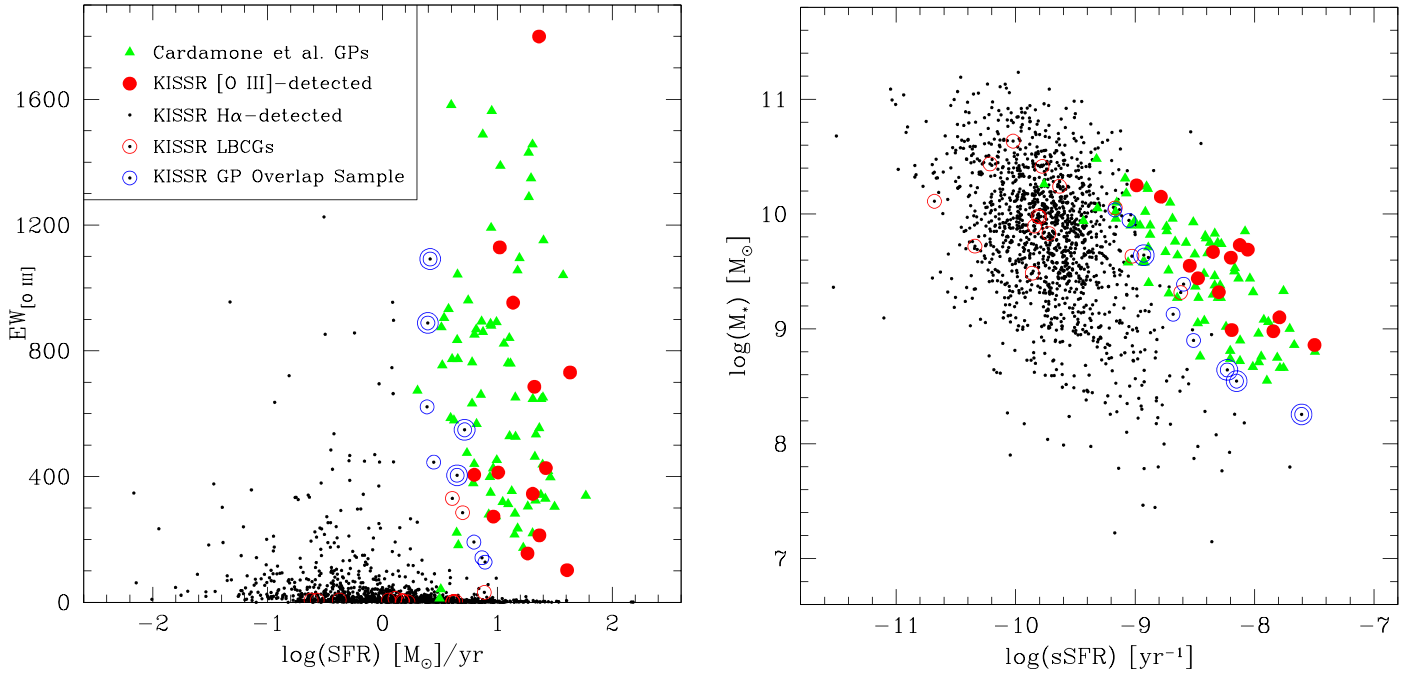

Figure 11. We reproduce Figures 5 and 6 and indicate the two subsamples of KISS galaxies discussed in Sections 6.1 and 6.2. The KISSR galaxies indicated by red circles are the LBCGs identified by Werk et al. (2004). Note that most of the LBCGs are located along the bottom of the left panel at low [O III] EW. Blue circles denote the low-redshift KISS galaxies that fall within the parameter space envelope defined by the Cardamone et al. (2009) GPs in all three comparison plots discussed in Section 3. Objects with double blue circles are low-redshift ($z < 0.09$) GP candidates.

1734 and KISSB 36 and 74. We consider these four objects to be low-redshift GP analogs. All four exhibit a strong violet color in the SDSS three-color images, earning them the nickname purple grapes. While their SDSS colors are similar to KISSR 1038 (Figure 3), the reason for the purple color is somewhat different. In the case of these low-z systems, the strong [O III] lines are located with the SDSS g band (mapped to blue), while the Hα line is transitioning into the SDSS i band (mapped to red), giving rise to the violet color. At even lower redshifts, the Hα line will fall entirely in the SDSS r band, with the [O III] lines still being located in the g band, resulting in a strong blue color (aka blue berries; Yang et al. 2017b; Hysu et al. 2018). This is the case for the starburst regions in the two lower-redshift KISS LBCGs in Figure 12.

The remaining low-redshift GP candidates are nearly all either clearly in interacting or merging systems or exhibiting morphological peculiarities indicative of a recent merger. Apparently, the star formation levels and spectral signatures exhibited in at least some merging systems are similar to those found in GP galaxies. We are not necessarily trying to draw a connection between the GPs and recent merger activity, since the GPs typically do not show evidence for such activity (e.g., no obvious tidal features). Nonetheless, the merger of two gas-rich systems represents a viable explanation for the extreme star formation activity found in GPs.

The four low-z GP candidates identified above are denoted in Figure 11 by double blue circles. Their properties are listed in Table 4, which presents much of the same information found in Tables 2 and 3 for the [O III]-detected KISS galaxies. Not surprisingly, the low-redshift GP candidates tend to be lower-luminosity and lower-mass galaxies compared to the [O III]-detected KISSR GPs. Three of the four have stellar masses lower than any of their higher-redshift counterparts. They also have metal abundances that are low for their luminosities, although they are not as extreme as the [O III]-detected KISS GPs in this regard. Three have very low star formation ages, with KISSB 74 being capable of forming its entire stellar population in only 40 Myr at its current SFR. Finally, these local GP candidates are not as extreme as the higher-redshift KISS GPs in terms of their starburst luminosity enhancements. While KISSR 715 and KISSB 74 both exhibit luminosity enhancements of $\sim$1.8 mag, KISSR 1734 has an enhancement of only 0.34 mag and a fraction of its luminosity coming from the current starburst of 27%.

The four KISS galaxies highlighted in Table 4 appear to represent low-redshift examples of the GP galaxies. They are all much less extreme than the [O III]-detected KISS GPs that are the subject of this paper. Whether they represent faded examples of the types of GPs seen at higher redshift or simply lower-mass examples (or a mix) remains to be determined. What is clear is that GP-like systems are present in the local universe at redshifts as low as $\sim$0.05.

6.3. What Do the Extreme GPs Look Like Today?

The discussion of the previous section at least partially answers the question of whether there are GP-like galaxies in the very local universe. We next consider the question of what the galaxies in the KISSR [O III]-detected GP sample might look like today. They are quite extreme in terms of their properties at $z \sim 0.3$–0.4. Furthermore, they must evolve substantially in the intervening 3–4 Gyr, since there do not appear to be any systems with such extreme properties at $z < 0.1$. If there were, they would stand out in wide-field redshift surveys like 2dF (Colless et al. 2001) and SDSS (Strauss et al. 2002).

Here we consider two possible evolutionary pathways for the KISSR [O III]-selected GPs. One possibility is that the galaxies seen as GPs at $z \sim 0.3$–0.4 are still compact, star-forming systems. In other words, they have retained some of their gas

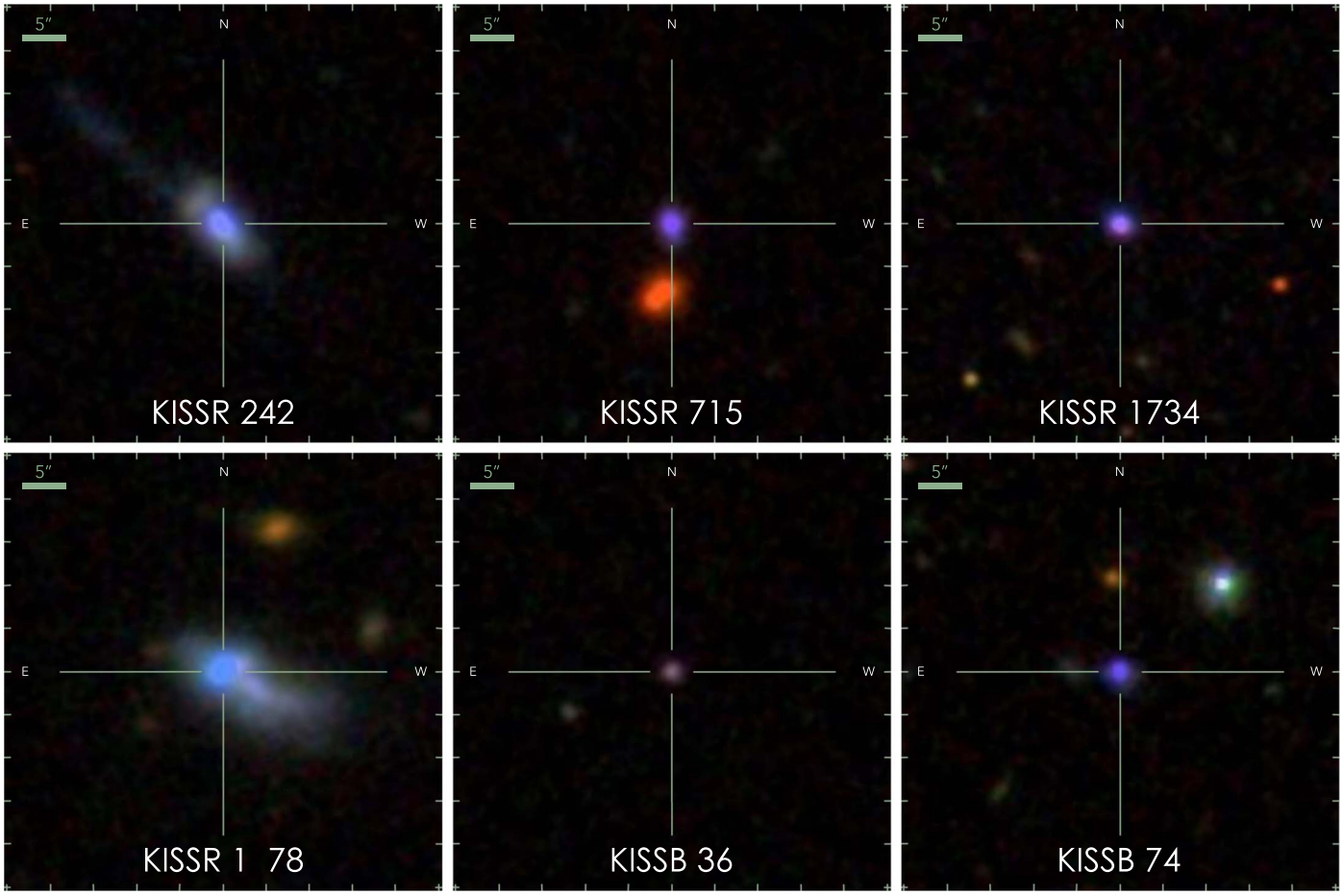

Figure 12. Left: SDSS images of two LBCGs (KISSR 242 and 1578) from the Werk et al. (2004) sample. Both LBCGs have a bright knot of star formation embedded in a more extended galaxy and display disturbed morphologies. Note the faint tidal feature extending above and to the left of KISSR 242. Middle and right: SDSS images of four galaxies from the KISSR 715 and 1734 and KISSB 36 and 74 SFG samples. These galaxies are found in the parameter space occupied by the Cardamone et al. (2009) GPs, and they have similar compact morphologies to the Cardamone et al. (2009) and KISSR GPs. The specific redshifts of these galaxies coupled with their strong emission lines result in their purple color (see text).

and are still making stars. However, we infer that their star formation activity would need to have dropped to a lower level than in the past, as mentioned above. Presumably, they would need to fade substantially, which, in turn, would imply substantially lower SFRs at the current time.

One of the lower-redshift KISSR galaxies may represent such an example of a faded GP. KISSR 1734 (Figure 12, Table 4) has a stellar mass comparable to those of the KISSR [O III]-detected GPs, a very compact morphology, and an SFR that is substantially lower than those exhibited by the higher-redshift GPs of similar mass (four to eight times lower than the four with similar masses). While KISSR 1734 was just bright enough to be included in the SDSS spectroscopic survey, systems with somewhat lower current SFRs and/or somewhat higher redshifts would likely have been missed by the currently available wide-field redshift surveys. Hence, one could imagine that a modest population of faded GPs, having morphologies similar to their higher-redshift counterparts, could exist in the local universe without attracting our attention.

The second possibility we consider is a scenario where the GPs seen at $z \sim 0.3$–0.4 have been totally quenched, presumably by a combination of using up their gas via star formation and gas removal via supernova explosions. In this case, the evolving GP would fade rather quickly. It is also likely that the system would assume a somewhat less compact configuration after the loss of its gas, although the degree to which the stellar component expands would probably not be too dramatic. Hence, we would imagine a centrally concentrated stellar system with a dominant 3–4 yr old stellar population.

In this scenario, the evolving GP galaxies may end up looking like compact E + A galaxies: stellar systems with an elliptical-like morphology with no current star formation but a strong spectral signature of a young stellar population (Zabludoff et al. 1996). Originally, E + A galaxies were thought to be formed in rich galaxy clusters, but they have also been found in the field and small groups (e.g., Zabludoff et al. 1996; Yang et al. 2008). A subsample of E + A galaxies with very compact morphologies has been recognized (Zahid et al. 2016). However, the Zahid et al. (2016) sample consists of galaxies with higher masses than the GPs. Because most known GPs are unresolved, it is hard to compare the relative sizes of the Zahid et al. (2016) compact E + A galaxies and GPs. It is possible that the postburst GP evolution represents a (probably minor) pathway to the formation of intermediate-mass compact E + A galaxies.

It is worth noting that the remnant GPs will likely not evolve substantially due to hierarchical merging. We are seeing them as compact, possibly young systems at $z = 0.3$–0.4 (and at lower redshifts in the Cardamone et al. 2009 sample). This is

Table 4
Properties of Low-redshift KISS GP Candidates

KISSR	KISSB	B_o	z	EW$_{[O\,III]}$ (Å)	M_B	log(M_*) ($M_\odot$)	log(O/H)+12	log(SFR) ($M_\odot$ yr^{-1})	SF Age (Myr)	SBE[a] (mag)	% SB Light
(1)	(2)	(3)	(4)	(5)	(6)	(7)	(8)	(9)	(10)	(11)	(12)
⋯	36	20.40	0.08874	888.7	−17.64	8.55	7.68	0.40	141	0.84	55.9
⋯	74	18.86	0.05575	404.1	−18.12	8.26	8.01	0.65	40	1.80	80.9
715	190	18.67	0.06815	1092.0	−18.79	8.64	7.72	0.42	169	1.83	81.5
1734	⋯	18.40	0.06568	548.7	−18.97	9.64	8.26	0.72	845	0.34	26.9

Note.
[a] SBE = starburst enhancement; see Section 4.

well past the epoch where galaxy growth due to accretion was efficient. Hence, it seems safe to assume that the GPs will not accrete enough material to evolve into, for example, disk galaxies, like we see in the local universe.

The precise method by which the GPs evolve may well depend on their local environments. Preliminary studies suggest that GPs tend to be located in low- and intermediate-density environments (Kurtz et al. 2016). Ongoing work by our group (S. W. Brunker et al. 2020, in preparation) is looking into the galaxian environments populated by GPs.

7. Conclusions

The primary focus of this paper has been to explore the properties and evolutionary status of the [O III]-selected SFGs identified by Salzer et al. (2009) from the KISSR ELG survey. While the bulk of the KISSR galaxies were detected via their Hα emission at low redshifts ($z < 0.095$), the [O III]-selected galaxies were detected in the redshift range 0.29–0.42 when strong [O III] λ5007 entered the KISSR spectral bandpass. We present new ground-based NIR and Spitzer MIR and FIR fluxes for members of this sample and derive essential properties such as stellar masses and SFRs.

We then compared the properties of the KISSR [O III]-detected galaxies with the color-selected GP galaxy sample from Cardamone et al. (2009) in order to assess the degree to which the galaxies in the two samples are similar. Parameters compared between the two samples include stellar mass, [O III] λ5007 EW, SFR, sSFR, and metallicity. We find that the properties of the KISSR [O III]-detected sample fully overlap those of the Cardamone et al. (2009) GPs. We conclude that the KISSR [O III]-detected galaxies are consistent with being drawn from the same population of galaxies as the Cardamone et al. (2009) GPs.

After ascertaining that the [O III]-detected KISSR SFGs are in fact GPs, we further explored their nature by comparing their properties to those of the KISSR Hα-detected SFGs. In addition to the comparisons mentioned above, we compared the B-band luminosities of the two samples, as well as their relative locations in MZ, LZ, and mass–luminosity diagrams. In all comparisons considered, the KISSR GPs stand out as being extreme.

Similar to results from studies of other samples of GPs, the KISSR GPs exhibit extremely high SFRs and sSFRs for their masses. Unlike some previous studies that have parameterized GPs as being dwarf galaxies, the KISSR GP sample extends to intermediate masses above 10^{10} $M_\odot$. The KISSR GPs are also metal-poor when compared to other galaxies of comparable luminosity or mass. They exhibit an extreme displacement from the KISSR Hα-detected galaxies in the LZ diagram. However, our analysis suggests that the offset in metal abundance is only 0.39 dex when the luminosity enhancement is accounted for. Our use of the mass–luminosity relation reveals that the [O III]-detected KISSR galaxies exhibit extreme starburst enhancements averaging 3.08 mag. That is, the KISSR GPs are, on average, a factor of 17 times brighter than a typical SFG of the same mass. This luminosity enhancement equates to 94% of the light coming from the starburst population.

One of the most astounding sets of numbers, from our perspective, are the extremely low star formation ages (i.e., inverse of the sSFR) for the KISSR GPs as a class. With ages as low as 31 Myr and a median age of 158 Myr, this parameter strongly suggests that these GPs are undergoing their first major episode of star formation. The existence of young galaxies in the nearby universe has been discussed and debated for years (e.g., Searle & Sargent 1972; Izotov & Thuan 2004; Mamon et al. 2020). In the case of the most extreme KISSR GP systems, it is hard to imagine that the observed starbursts are part of the ongoing evolution of an otherwise normal galaxy. In any case, the short formation timescales for GPs implies that they would be natural sources of escaping ionizing radiation in the early universe, since their evolutionary ages nicely coincide with the young age of the universe during the epoch of reionization.

We calculated the number density of the KISSR GPs to be 1.35×10^{-6} Mpc^{-3}, which shows that GPs are extremely rare. We predict that there should be 0.70 GPs in the volume covered by the low-redshift KISSR Hα-detected survey. We used the KISSR Hα-detected catalog to look for GP analogs in the local universe ($z < 0.1$). We found four GP analogs that have properties that overlap with the Cardamone et al. (2009) GPs and similar compact morphologies as the GPs. These analogs are less extreme in their properties compared with the KISS GPs, but they show that GP-like systems are present in the local universe. At least one of these may represent a faded version of the more extreme GPs seen at intermediate redshifts.

We acknowledge financial support from the National Science Foundation for the KISS project, as well as for the subsequent follow-up spectroscopy campaign (NSF-AST-9553020, NSF-AST-0071114, and NSF-AST-0307766). We are grateful to the Indiana University College of Arts and Sciences for their continued support of the WIYN Observatory. We thank the staff of the WIYN Observatory for their excellent support during both our WHIRC NIR imaging observations and our Hydra spectroscopic runs. This work is based in part on observations made with the Spitzer Space Telescope, which was operated by the Jet Propulsion Laboratory, California Institute of Technology, under a contract with NASA. This

publication makes use of data products from the Wide-field Infrared Survey Explorer (WISE), which is a joint project of the University of California, Los Angeles, and the Jet Propulsion Laboratory/California Institute of Technology, funded by the National Aeronautics and Space Administration. Funding for the SDSS has been provided by the Alfred P. Sloan Foundation, the Participating Institutions, the National Science Foundation, the U.S. Department of Energy, the National Aeronautics and Space Administration, the Japanese Monbukagakusho, the Max Planck Society, and the Higher Education Funding Council for England. The SDSS website is http://www.sdss.org/. The SDSS is managed by the Astrophysical Research Consortium for the Participating Institutions. The Participating Institutions are the American Museum of Natural History, the Astrophysical Institute Potsdam, the University of Basel, the University of Cambridge, Case Western Reserve University, the University of Chicago, Drexel University, Fermilab, the Institute for Advanced Study, the Japan Participation Group, Johns Hopkins University, the Joint Institute for Nuclear Astrophysics, the Kavli Institute for Particle Astrophysics and Cosmology, the Korean Scientist Group, the Chinese Academy of Sciences (LAMOST), Los Alamos National Laboratory, the Max Planck Institute for Astronomy (MPIA), the Max Planck Institute for Astrophysics (MPA), New Mexico State University, Ohio State University, the University of Pittsburgh, the University of Portsmouth, Princeton University, the United States Naval Observatory, and the University of Washington.

Facilities: WIYN (Hydra and WHIRC), Spitzer, WISE.

ORCID iDs

Samantha W. Brunker https://orcid.org/0000-0001-6776-2550
John J. Salzer https://orcid.org/0000-0001-8483-603X
Steven Janowiecki https://orcid.org/0000-0001-9165-8905
Rose A. Finn https://orcid.org/0000-0001-8518-4862
George Helou https://orcid.org/0000-0003-3367-3415

References

Baldwin, J. A., Phillips, M. M., & Terlevich, R. 1981, PASP, 93, 5
Bell, E. F., & de Jong, R. S. 2001, ApJ, 550, 212
Bell, E. F., McIntosh, D. H., Katz, N., et al. 2003a, ApJS, 149, 289
Bell, E. F., McIntosh, D. H., Katz, N., et al. 2003b, ApJ, 585, 117
Bergvall, N., Marquart, T., Way, M. J., et al. 2016, A&A, 587, 72
Bruzual, G., & Charlot, S. 2003, MNRAS, 344, 1000
Cardamone, C., Schawinski, K., Sarzi, M., et al. 2009, MNRAS, 399, 1191
Cardelli, J. A., Clayton, G. C., & Mathis, J. S. 1989, ApJ, 345, 245
Colless, M., Dalton, G., Maddox, S., et al. 2001, MNRAS, 328, 1039
Dale, D. A., Helou, G., Magdis, G. E., et al. 2014, ApJ, 784, 83
de Lapparent, V., Geller, M. J., & Huchra, J. P. 1989, ApJ, 343, 1
Efstathiou, G., Ellis, R. S., & Peterson, B. A. 1988, MNRAS, 232, 431
Faber, S. M., Willmer, C. N. A., Wolf, C., et al. 2007, ApJ, 665, 265
Fan, X., Strauss, M. A., Becker, R. H., et al. 2006, AJ, 132, 117
Finn, R. A., Desai, V., Rudnick, G., et al. 2010, ApJ, 720, 87
Gronwall, C., Jangren, A., Salzer, J. J., et al. 2004a, AJ, 128, 644
Gronwall, C., Salzer, J. J., Sarajedini, V. L., et al. 2004b, AJ, 127, 1943
Guzmán, R., Östlin, G., Kunth, D., et al. 2003, ApJL, 586, L45
Haiman, Z., & Loeb, A. 1998, ApJ, 503, 505
Henry, A., Scarlata, C., Martin, C. L., et al. 2015, ApJ, 809, 19
Hirschauer, A. S., Salzer, J. J., Janowiecki, S., et al. 2018, AJ, 155, 82
Hogg, D. W., Baldry, I. K., Blnaton, M. R., et al. 2002, arXiv:astro-ph/0210394
Hoyos, C., Koo, D. C., Phillips, A. C., et al. 2005, ApJL, 635, L21
Hysu, T., Cooke, R. J., Prochaska, J. X., et al. 2018, ApJ, 863, 134
Inoue, A. K. 2011, MNRAS, 415, 2920
Izotov, Y. I., Guseva, N. G., & Thuan, T. X. 2011, ApJ, 728, 161
Izotov, Y. I., Orlitová, I., Schaerer, D., et al. 2016a, Natur, 529, 178
Izotov, Y. I., Schaerer, D., Thuan, T. X., et al. 2016b, MNRAS, 461, 3683
Izotov, Y. I., Schaerer, D., Worseck, G., et al. 2018a, MNRAS, 474, 4514
Izotov, Y. I., Schaerer, D., Worseck, G., et al. 2020, MNRAS, 491, 468
Izotov, Y. I., & Thuan, T. X. 2004, ApJ, 616, 768
Izotov, Y. I., Thuan, T. X., & Guseva, N. G. 2017, MNRAS, 471, 548
Izotov, Y. I., Worseck, G., Schaerer, D., et al. 2018b, MNRAS, 478, 4851
Jangren, A., Salzer, J. J., Sarajedini, V. L., et al. 2005a, AJ, 130, 2571
Jangren, A., Wegner, G., Salzer, J. J., et al. 2005b, AJ, 130, 496
Janowiecki, S., & Salzer, J. J. 2014, ApJ, 793, 109
Janowiecki, S., Salzer, J. J., van Zee, L., et al. 2017, ApJ, 836, 128
Jaskot, A. E., Dowd, T., Oey, M. S., et al. 2019, ApJ, 885, 96
Jaskot, A. E., & Oey, M. S. 2013, ApJ, 766, 91
Jaskot, A. E., Oey, M. S., Scarlata, C., et al. 2017, ApJL, 851, L9
Kakazu, Y., Cowie, L. L., & Hu, E. M. 2007, ApJ, 668, 853
Kennicutt, R. C., Jr. 1983, ApJ, 272, 54
Kennicutt, R. C., Jr. 1998, ARA&A, 36, 189
Kurtz, H., Jaskot, A., Drew, P., et al. 2016, AAS Meeting Abstracts, 227, 234.02
Madau, P., & Haardt, F. 2015, ApJL, 813, L8
Madau, P., Rees, M. J., Volonteri, M., et al. 2004, ApJ, 604, 484
Mamon, G. A., Trevisan, M., Thuan, T. X., et al. 2020, MNRAS, 492, 1791
McGreer, I. D., Mesinger, A., & D'Odorico, V. 2015, MNRAS, 447, 499
McQuinn, K. B. W., Skillman, E. D., Cannon, J. M., et al. 2010, ApJ, 724, 49
Meixner, M., Smee, S., Doering, R. L., et al. 2010, PASP, 122, 451
Melbourne, J., & Salzer, J. J. 2002, AJ, 123, 2302
Nakajima, K., & Ouchi, M. 2014, MNRAS, 442, 900
Noll, S., Burgarella, D., Giovannoli, E., et al. 2009, A&A, 507, 1793
Panter, B., Heavens, A. F., & Jimenez, R. 2004, MNRAS, 355, 764
Pence, W. 1976, ApJ, 203, 39
Rivera-Thorsen, T. E., Hayes, M., Östlin, G., et al. 2015, ApJ, 805, 14
Robertson, B. E., Ellis, R. S., Dunlop, J. S., et al. 2010, Natur, 468, 49
Salpeter, E. E. 1955, ApJ, 121, 161
Salzer, J. J., Gronwall, C., Lipovetsky, V. A., et al. 2000, AJ, 120, 80
Salzer, J. J., Gronwall, C., Lipovetsky, V. A., et al. 2001, AJ, 121, 66
Salzer, J. J., Gronwall, C., Sarajedini, V. L., et al. 2002, AJ, 123, 1292
Salzer, J. J., Jangren, A., Gronwall, C., et al. 2005a, AJ, 130, 2584
Salzer, J. J., Lee, J. C., Melbourne, J., et al. 2005b, ApJ, 624, 661
Salzer, J. J., Williams, A. L., & Gronwall, C. 2009, ApJL, 695, L67
Searle, L., & Sargent, W. L. W. 1972, ApJ, 173, 25
Skrutskie, M. F., Cutri, R. M., Stiening, R., et al. 2006, AJ, 131, 1163
Strauss, M. A., Weinberg, D. H., Lupton, R. H., et al. 2002, AJ, 124, 1810
Veilleux, S., & Osterbrock, D. E. 1987, ApJS, 63, 295
Verhamme, A., Orlitová, I., Schaerer, D., et al. 2017, A&A, 597, A13
Walcher, J., Groves, B., Budavári, T., et al. 2011, Ap&SS, 331, 1
Wegner, G., Salzer, J. J., Jangren, A., et al. 2003, AJ, 125, 2373
Werk, J. K., Jangren, A., & Salzer, J. J. 2004, ApJ, 617, 1004
Wright, E. L., Eisenhardt, P. R. M., Mainzer, A. K., et al. 2010, AJ, 140, 1868
Yang, H., Malhotra, S., Gronke, M., et al. 2017a, ApJ, 844, 171
Yang, H., Malhotra, S., Rhoads, J. E., et al. 2017b, ApJ, 847, 38
Yang, Y., Zabludoff, A. I., Zaritsky, D., et al. 2008, ApJ, 688, 945
York, D. G., Adelman, J., Anderson, J. E., et al. 2000, AJ, 120, 1579
Zabludoff, A. I., Zaritsky, D., Lin, H., et al. 1996, ApJ, 466, 104
Zahid, H. J., Baeza Hochmuth, N., Geller, M. J., et al. 2016, ApJ, 831, 146